BOSTON UNIVERSITY
GRADUATE SCHOOL

Dissertation

KINETIC PROPERTIES OF STOCHASTIC PROCESSES

by

ELY BEN-NAIM
B.Sc., Hebrew University of Jerusalem, 1990

Submitted in partial fulfillment of the
requirements for the degree of
Doctor of Philosophy
1994

Approved by

First Reader

Sidney Redner, Ph.D.
Professor of Physics

Second Reader

Ganapathy Murthy, Ph.D.
Assistant Professor of Physics

to Ellen

ACKNOWLEDGMENTS

I would like to express my deepest gratitude to Sidney Redner, my thesis advisor. He has used his experience and knowledge to direct me to positive and creative avenues. He has engrained in me the lesson of seeking the beauty in science. I am also thankful for Sid's sincerity, patience and kindness.

I was fortunate to work with Paul Krapivsky over the past year, and I would like to thank him for all that he has taught me and for his friendship. I am grateful that I had the opportunity to collaborate with Daniel ben-Avraham, Francois Leyvraz, George Weiss and Jun Zhuo. I have enjoyed scientific discussions with Ronald Dickman, Alon Drory, Shlomo Havlin, Hernan Lerralda, Vladimir Privman, Stefan Schwartzer Haim Taitelbaum, Julian Talbot, Bill Young, Martin Vilela and Hwang Won Muk.

My stay in Boston would have never been the same without the friendship of Bill Hellman, Townsend Zwart, Ned Greene, Steve Harrington, Balaji Bashayam, Klaus Breuer and Monish Varma.

I would like to thank all my teachers, from elementary school through the Hebrew University. Special thanks to my High School Science teachers, Professor Levine and Professor Lipman for stimulating my interest in the Physical Sciences.

Last but not least, I thank my parents, Salomon and Simi, my siblings, Dina, Johnny and Alex and my neice, Lidi, for their love and for supporting me from afar.

I dedicate this thesis to Ellen, my wonderful wife, for being there for me and for her love.

KINETIC PROPERTIES OF STOCHASTIC PROCESSES

(Order No.)

ELY BEN-NAIM

Boston University Graduate School, 1994

Major Professor: Sidney Redner, Professor of Physics

ABSTRACT

In this thesis, kinetic and steady state properties of a range of stochastic and nonequilibrium models are investigated. A typical process is specified by a transport mechanism and a reaction mechanism and this leads naturally to simple "toy-like" models.

In the first part, the kinetics of ballistically-controlled reactions with continuous initial particle velocity distributions are studied. A non-universal power-law decay is found for both the concentration and the velocity, with the characteristic exponents governed by the form of the initial velocity distribution. For the case where particles annihilate upon contact, a mean-field theory provides good estimates for the decay kinetics. A ballistic aggregation model, inspired by one-lane traffic flows, is solved and the qualitative behavior of the reaction process is determined. The contribution of diffusion to the annihilation process with a bimodal initial velocity distribution is also studied. Using scaling arguments and series analysis techniques, it is shown that introduction of diffusion, even if small, alters the asymptotic behavior of the concentration of particles.

In the second part, a steady state model of the inhomogeneous two-species annihilation reaction, $A + B \to 0$, is presented. In this model, two different species A and B are injected with equal fluxes at the opposite boundaries of a finite system. Analytical results for the concentration profile are obtained by solving the reaction-diffusion equations. The dependence of the reaction rate on the flux is found and this result is applied to the time-dependent reaction model.

In the third part, collective properties of adsorption-desorption models in one dimension are studied. The steady state of a reversible parking process, where monodisperse particles adsorb and desorb on a one-dimensional substrate, is solved. The system exhibits a weak dependence on the adsorption rate in the desorption-controlled regime. To understand this behavior, an irreversible model incorporating immediate adsorption as well as desorption is introduced. A slow approach to the fully occupied state is found by heuristic arguments and by simulations. Furthermore, a cluster approximation technique is suggested to analyze the critical nature of a one-dimensional irreversible adsorption-desorption model.

Contents

List of Figures

List of Tables

Chapter 1

Introduction

"Would I find the complete many-body wave function, I would not know what to do with it" said Richard Feynman. This famous quote sums up my perspective of the essence of modern physics. To write a microscopic function that describes 10^{23} particles explicitly, a page larger than the sun-to-earth distance is required, thereby making such an approach of little practical use. Conceptual understanding of a physical system is necessary for making measurable predictions rather than obtaining a multivariative description of a many-particle system.

Disagreeing with Einstein's celebrated quote, I believe God's favorite toy is indeed the dice. Nature is often represented by stochastic terms. The quantum mechanical description of particles is essentially derived from probability amplitudes, which determine the likelihood of finding a particle at a certain point in time and space. Randomness governs not only quantum systems but also classical systems. The same mechanism that governs earnings in a dice throwing game controls the propagation of heat. As a result, heat propagates considerably slower in comparison with light.

Probabilistic descriptions are especially well-suited for analyzing many-particle phenomena. According to the central limit theorem, the statistical uncertainty diminishes as the number of random variables is increased. This uncertainty additionally diminishes when average macroscopic properties are calculated. Thus, it proves useful to study the limit of an infinite number of particles.

In this thesis, I study interacting particle systems by analyzing their underlying stochastic processes. A typical process is specified by a transport mechanism and an interaction mechanism, and this approach leads naturally to simple "toy-like" models. I focus on reaction processes and adsorption processes using mainly classical theoretical methods which are supported by computational studies. In addition, I present new theoretical methods and analysis techniques to investigate certain problems for which the conventional methods are not applicable.

In most of the problems we consider, time dependent phenomena are of interest, while in the remainder steady-state properties are important as well. In either situation, the asymptotic analysis of a properly defined microscopic process provides the desired physical insight. Generally, most details associated with the initial configuration vanish after waiting long enough or equivalently, become irrelevant as averaging procedures take place. Hence, we view the long time behavior as a tool for classifying processes into universality classes, *i. e.*, families that obey similar physics.

Generally, exact theoretical analysis is possible in the one-dimensional case only. However, one can project the understanding obtained for such soluble problems into a theory that holds in an arbitrary dimension. Scaling techniques are powerful in that respect, since they require a minimal amount of details and labor. In sufficiently high dimensions, our systems are expected to match a "mean-field" like behavior. To formulate such a theory we typically assume that all particles are neighbors of each other. This assumption yields a dimension-independent theory that ignores any spatial structures or microscopic fluctuations. The resulting deviation between the actual properties and the mean-field theory measures the extent to which particle interact. Specifically, because of effective repulsions between the particles our reactive systems exhibit anomalously slow kinetics. To a certain extent, a reacting particle system organizes itself such that the number of remaining reactants is maximized.

In equilibrium transitions between different states of the system obey the detailed balance condition that the flux between any two microscopic configurations of the system vanish. An equilibrium process also requires such transition rates to be microscopically reversible. Some of the adsorption processes we study are irreversible and hence, they are far from equilibrium. Not all possible configurations are accessible, resulting in significantly different steady state and kinetic properties than their equilibrium counterparts. In addition, collective behavior of the adsorbants cause slower than mean field approach to the steady state.

In chapter 2, a short review of some elementary kinetic processes is presented. The purpose of this mostly self-contained presentation is to place the work we have done in proper context and also to provide theoretical background. The starting point is a time-dependent solution of the Ising chain. We make use of the isomorphism between the spin system and annihilating random walkers to solve both processes. The correspondence between the slow decay kinetics of the diffusive single-species annihilation process and the Ising chain at its zero temperature critical point is established. Also, reversible adsorption is mapped to the equilibrium spin model at arbitrary temperature. Steady state properties are compared with the irreversible adsorption case, exemplifying the role of reversibility.

In chapters 3–5, the kinetics of reaction processes with ballistic particles are studied. Such a process can describe charged exciton recombination kinetics in an external electric field. The single species annihilation process, $A + A \to 0$, and the aggregation process, $A + A \to A$, with a continuous initial particle velocity distribution are studied. For the annihilation case, time-dependent properties of the concentration of particles and the typical velocity in one and two dimensions are investigated. A non-universal power-law decay is found for both the concentration and the velocity, in which the characteristic exponents, are governed by the form of the initial velocity distribution. Using scaling techniques and numerical integration of the Boltzmann equation, the exponents of the power law decay are estimated. Monte Carlo simulations of the process are performed and good agreement with the mean-field predictions is found.

The aggregation process, motivated by one-lane traffic flows, is useful in explaining the non-universal decays found for the annihilation model. Here aggregates move with a velocity equal to the minimal particle velocity, and thus, statistics of extremes govern this process. Asymptotically exact expressions are obtained for the velocity distribution and the joint mass-velocity distribution. Although the actual quantitative behavior of the ballistic aggregation and annihilation processes are different, both exhibit the same functional dependence on the initial conditions. Generalization of this model to situations with input and to spatially inhomogeneous situations are formally solved. For the input case, a transition to a steady state is also found as the input velocities are varied.

The contribution of diffusion to the annihilation process with a bimodal initial velocity distribution is also studied. Using scaling arguments, we show that introduction of diffusion, even if small, alters the asymptotic behavior of the concentration of particles. To confirm this prediction, a new general analysis method is developed. The approach is based on using an enumeration of all states to determine the exact time evolution of a reactive system. A Padé analysis technique is suggested for obtaining the asymptotic behavior of a process from its short-time Taylor series. This method is applied to ballistic annihilation problem with superimposed diffusion and the result of the scaling approach is verified.

In chapter 6, a steady state model of the inhomogeneous two-species annihilation reaction, $A + B \to 0$, is presented. This reaction scheme is relevant to studying electron-hole annihilation in irradiated semiconductors, for example. In our model, two different species A and B are injected with equal flux at the opposite boundaries of a finite system. The transport mechanism is diffusive and annihilation occurs when two different species meet. Analytical results for the concentration profile are obtained by solving the reaction-diffusion equations. The dependence of the reaction rate on the flux is found, and this result is applied to the time-dependent reaction model. The local reaction rate exhibits a transition from maximum near the boundary to maximum in the center of the system as the flux is increased. The solution technique is applied to systems with radial geometries in two- and three-dimensions as well.

In chapters 7 and 8, collective properties of adsorption-desorption models in one dimension are studied. A reversible parking process where monosize particles adsorb on a substrate is suggested for modeling binding of protein macromolecules on a surface. Exact results for the density and the distribution function of empty intervals in the steady-state are obtained. The system exhibits a weak dependence on the adsorption rate in the desorption-controlled regime. To understand this behavior, an irreversible model incorporating immediate adsorption as well as desorption is introduced. A slow approach to the fully occupied state is found by heuristic arguments, and this behavior is confirmed by Monte-Carlo simulations.

In chapter 8, an approximate solution to the contact process is developed. In this lattice model, particles desorb homogeneously and adsorb near occupied sites only. Such an autocatalytic reaction is closely related to surface oxidation of carbon monoxide on metal surfaces. This nonequilibrium process possesses an absorbing state and exhibits a continuous phase transition between an active state and an absorbing state. Such phase transitions are characterized by nontrivial critical exponents. In our approximation scheme, the correlation between two empty intervals is neglected. This approach yields different critical behavior, namely, a first order phase transition. However, for a significant range of desorption rates, the density and the gap distribution, that arises from our theory approximates the actual process accurately. Moreover, the values of the transition point and the critical exponents are close to the values found by series expansion techniques.

Chapter 2

Review

To put the work presented in this thesis in perspective, I present a short review of simple stochastic processes in this chapter. I begin with perhaps the simplest microscopic process modeling a chemical reaction, diffusive-driven single species annihilation. This process can be analyzed by considering the kinetic Ising model at zero temperature and identifying domain walls with particles. The classical solution, obtained by Glauber, is outlined as a starting point and used to derive the solution to the annihilation model. This correspondence establishes a deep relation between the spin model as a stochastic process and the collective properties of many interacting random walkers.

Moreover, the finite temperature Ising model can be mapped to a reversible adsorption model. The equilibrium Ising model solution yields, with a suitably defined temperature, a steady state solution to the adsorption process. Irreversible adsorption is then introduced and used to explain the significance of reversibility in kinetic processes.

Some of the most interesting phenomena in nonequilibrium physics are induced by fluctuations. In applications to chemical reactions, a striking example is the two species annihilation process. We describe the solution to a ballistically-driven reaction and stress the role of the initial density fluctuations in the asymptotic limit. This argument can be repeated for obtaining a scaling solution to the two species annihilation model. It is shown that slow kinetics take place as a result of the formation of single species domains.

2.1 The Kinetic Ising Model

One of simplest interacting particles system, the spin 1/2 model suggested by Ising [1], successfully describes the ferromagnetic phase transition [2]. In this model the interaction between nearest neighbors only is taken into account according to the following Hamiltonian,

$$H = -J\sum_i \sigma_i\sigma_{i+1}, \tag{2.1}$$

written explicitly for one dimension, with $\sigma_i = \pm 1$. When the spins are coupled to a heat reservoir, the equilibrium properties are unique, given the energy function of Eq. (2.1). The non-equilibrium behavior, however, depends on the dynamic leading the system to equilibrium and is generally not well defined. To define the time-dependent process, the transition rates between possible states of the system need to be specified. One can introduce sequential dynamics, *i. e.*, spins can change only one at a time. This yields a Markoff process, and taking these rates according to the detailed balance requirements of the equilibrium state allows a solution [3].

A many-spin system can be generally described by the collective probability function $P(\{\sigma\},t) \equiv P(\{\sigma_1,\ldots,\sigma_N\},t)$. When the individual spins, σ_i, undergo a spin-flip with rate $w_i(\sigma_i)$, the collective probability obeys the following rate equation,

$$\frac{\partial P(\{\sigma\},t)}{\partial t} = -\left(\sum_i w_i(\sigma_i)\right) P(\{\sigma\},t) + \sum_i w_i(-\sigma_i)P(\{\sigma_1,\cdots-\sigma_i,\cdots\sigma_N\},t). \tag{2.2}$$

The negative term represents loss of probability due to all possible transitions out of the state $\{\sigma\}$, while the gain term is obtained by noting that only configurations differing from $\{\sigma\}$ by one spin exactly contribute. One can check that summation of the rate equations over all possible states yields zero, since the total probability is conserved. We are interested in the evolution of average quantities such as the average spin value $\langle\sigma_i(t)\rangle = \sum_{\{\sigma\}} \sigma_i P(\{\sigma\},t)$ and the two-spin correlations $\langle r_{i,j}(t)\rangle =$

$\sum_{\{\sigma\}} \sigma_i \sigma_j P(\{\sigma\}, t)$. The rate equation for the single spin correlation is given by a summation of Eq. (2.2),

$$\frac{\partial \langle \sigma_i(t) \rangle}{\partial t} = \langle \sigma_i(t) w_i(\sigma_i(t)) \rangle. \tag{2.3}$$

Similarly, the pair correlation function satisfies the rate equation

$$\frac{\partial \langle \sigma_i(t) \sigma_j(t) \rangle}{\partial t} = -2 \langle \sigma_i(t) \sigma_j(t) \left[w_i(\sigma_i(t)) + w_j(\sigma_j(t)) \right] \rangle. \tag{2.4}$$

To define the dynamics, the flip rates have to be specified. In analogy with the bilinear form of the Hamiltonian function, and under the assumption that the rates depend only on the values of the nearest neighbor spins, the following form was postulated by Glauber*

$$w_i(\sigma_i) = \frac{\alpha}{2} \left[1 - \frac{\gamma}{2} \sigma_i (\sigma_{i-1} + \sigma_{i+1}) \right]. \tag{2.5}$$

These rates represent a tendency towards parallel spin alignment, for positive γ. In equilibrium, the probability that the system is in state $\{\sigma\}$ is given by the Boltzmann factor $\exp(-H(\{\sigma\})/k_B T)$, with k_B the Boltzmann constant and T the temperature. In addition, the equilibrium transition rates have to satisfy the detailed balance condition, namely, the flux between any two microscopic states of the system cancels. Therefore one finds

$$\frac{w_i(\sigma_i)}{w_i(-\sigma_i)} = \frac{p_i(-\sigma_i)}{p_i(\sigma_i)} = \exp\left(J \sigma_i (\sigma_{i-1} + \sigma_{i+1}) / k_B T \right). \tag{2.6}$$

This relation is always fulfilled when the two neighboring spins are anti-parallel, while when they are parallel, the relation $(1+\gamma)/(1-\gamma) = \exp(4J/kT)$ is satisfied. After a simple manipulation, one finds

$$\gamma = \tanh(2J/k_B T). \tag{2.7}$$

Note that the prefactor α is arbitrary, since it enters through a mere scaling of the time variable. Indeed, a positive coupling constant J yields a positive γ, and therefore the spin system is derived towards a ferromagnetic state.

---

*The most general reflection-invariant bilinear form is actually $w_i(\sigma_i) = (\alpha/2)(1+\delta\sigma_{i-1}\sigma_{i+1})(1-(\gamma/2)\sigma_i(\sigma_{i-1}+\sigma_{i+1}))$, and Eq. (2.5) was chosen for simplicity.

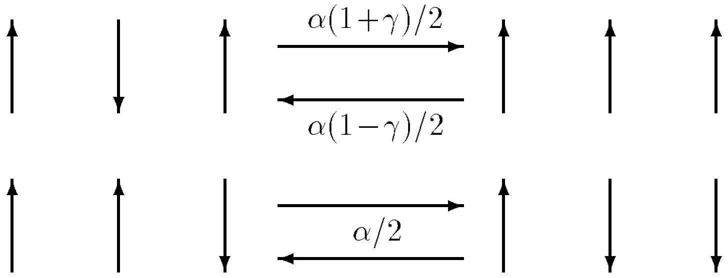

Figure 2.1: The spin flip process

We are now in a position to write the explicit equations satisfied by the spin correlation function. The suggested form for the rates has the advantage that a closed set of equations emerges. We will concentrate on the pair correlations since it gives physical insight and understanding of both the kinetics and the non-equilibrium properties. We restrict ourself to the spatially homogeneous situation, where the spin correlation depends only on the distance between the two spins. Hence, we write $r_k(t) = \langle\sigma_i(t)\sigma_{i+k}(t)\rangle$. Using Eqs. (2.4) and (2.5), the rate equation is obtained as

$$\frac{\partial r_k(t)}{\partial(\alpha t)} = -2r_k(t) + \gamma\left(r_{k-1} + r_{k+1}\right) \qquad k \neq 0. \tag{2.8}$$

Curiously, the pair correlation satisfies a continuous-time discrete-space random walk differential equation with an annihilation rate $2(1-\gamma)$. Under the general initial conditions $r_k(0)$ and the boundary condition $r_0 = 1$, the pair correlation function takes the form, derived using generating functions in Appendix A,

$$r_k(t) = \eta^k + \sum_{l=1}\left(r_l(0) - \eta^l\right)\left(I_{k-l}(2\alpha\gamma t) - I_{k+l}(2\alpha\gamma t)\right), \tag{2.9}$$

with $\eta = (1-\sqrt{1-\gamma^2})/\gamma = \tanh(J/kT)$.

The equilibrium solution $r_k^{eq} = \eta^k$ can be tacitly written in an exponential form,

$$r_k^{eq} = \exp(-k/\xi). \tag{2.10}$$

The constant ξ is readily identified as the correlation length, the spatial extent over which the spins are correlated. One can view this parameter as the typical size over which all spins are parallel. At the phase transition point, this length diverges. In the one-dimensional case, the critical temperature is zero, as seen from the relation $\xi = -1/\ln\ \tanh(J/kT)$. For finite temperatures, there is a finite correlation, indicating a paramagnetic behavior. In the limit of infinite temperature, the correlation length vanishes, and similarly the magnetization approaches zero.

The divergence of the correlation length is indicative of a critical slowing down mechanism, which can be seen by analyzing the temporal decay of the total magnetization. This quantity can be found by fixing one spin and summing over all correlations, (see Appendix A),

$$m(t) = m(0)\exp(-t/\tau) \qquad \text{with} \qquad \tau = \frac{1}{2\alpha(1-\gamma)} \tag{2.11}$$

As the system approaches the critical point, $\gamma \to 1$, the relaxation time τ diverges. This behavior is typical for systems at their transition point. Exponential temporal decay gives way to a slower power-law behavior. The nearest-neighbor correlation function, r_1, which is proportional to the average energy of the system, provides an example of such behavior. For simplicity, we consider the totally antiferromagnetic initial conditions, namely, $r_l(0) = (-1)^l$. Evaluating Eq. (2.9) under these initial conditions at zero temperature $\gamma = \eta = 1$ yields

$$r_1(t) = 1 - 2\exp(-2\alpha t)I_0(2\alpha t). \tag{2.12}$$

Since the modified Bessel functions have the asymptotic form $I_n(x) \sim e^x/\sqrt{2\pi x}$, the exponential factor cancels. One finds asymptotically, $1 - r_1(t) \sim (\pi\alpha t)^{-1/2}$. A power-law decay takes place at zero temperature, reminiscent of the general kinetic properties of systems at the critical point. This observation is significant to our studies, since we are mainly interested in kinetics of critical systems.

2.2 Diffusive Single-Species Annihilation

The model $A + A \to 0$ describes a chemical reaction in which diffusing particles annihilate upon contact [4, 5]. Diffusion is modeled by nearest-neighbor random walk, namely, particles hop with rate D to any nearest-neighbor site. An attempt to

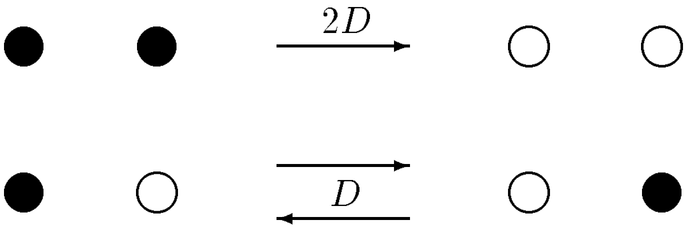

Figure 2.2: Single species annihilation

land on an occupied site results in an annihilation event, as illustrated in Figure 2.2. The annihilation process occurs with a rate $2D$ since a hopping attempt of either particle in the correct direction enables a reaction. The kinetic Ising model at zero temperature can be mapped into this stochastic process by identifying antiparallel spins with particles and conversely, parallel ones with empty sites. For example, the spin configuration $\cdots\downarrow\uparrow\uparrow\downarrow\cdots$ corresponds to the particle configuration $\cdots AOA\cdots$. The annihilation process $AA\to OO$ corresponds to the spin flip process $\uparrow\downarrow\uparrow\to\uparrow\uparrow\uparrow$, and the forbidden creation process $OO\to AA$ corresponds to $\uparrow\uparrow\uparrow\to\uparrow\downarrow\uparrow$. To establish the isomorphism between the particle and the spin processes, the corresponding rates are matched. With the help of Figures 2.1 and 2.2, one has $\alpha(1+\gamma)/2 = 2D$ and $\alpha(1-\gamma)/2 = 0$, or equivalently, $\alpha = 2D$ and $\gamma = 1$. Note also that the hop process rate D matches the rate $\alpha/2$, which describes spin-flips that do not change the energy. At zero temperature, energy raising transitions are forbidden ($\gamma = 1$) or equivalently, no creation of particles are allowed in the particle process. The particle concentration, $c(t)$, equals the domain boundary concentration, and from the definition of the nearest neighbor correlation, one finds

$$c(t) = \frac{1-r_1(t)}{2}. \tag{2.13}$$

Thus, the antiferromagnetic initial condition discussed in the previous section corresponds to the completely filled initial state. Finally, the time dependent concentration is found by substituting the proper rates in Eq. (2.11) to yield

$$c(t) = I_0(4Dt)\exp(-4Dt). \tag{2.14}$$

Interestingly, this concentration equals the probability that the displacement of a single random walk, hopping with rate $2D$, vanishes at time t. This can be partially understood by noting that the distance between two identical random walks itself executes a random walk with a hopping rate $2D$. In the long time limit, $t \gg 1/D$, the concentration shows a power law decay,

$$c(t) \sim (8\pi Dt)^{-1/2}. \tag{2.15}$$

Going back to $T = 0$ kinetic Ising model, the domain boundaries can be viewed as performing a random walk. When two domains meet, an annihilation event occurs and a combined larger domain form. The annihilating random walk argument sheds light on the behavior of the spin system.

We present now a heuristic argument that reproduces the above asymptotic result and which can also be easily generalized to higher dimensions. Let us assume that at given time, there exist an "interaction length", l, such that particles initially separated by a distance smaller than l have had a chance to interact (annihilate). Space can be divided now into "blocks" of volume l^d, and under this interaction length assumption, the number of surviving particles in each such block can be taken as one. The concentration is, thus, given by $c \sim l^{-d}$. Since the transport mechanism is diffusive, it is reasonable to assume that the interaction length is given by the average spread of a diffusive particle, $l \sim \sqrt{Dt}$. By substituting the time dependent length into the expression describing the concentrations we obtain

$$c(t) \sim (Dt)^{-d/2}. \tag{2.16}$$

Note that the concentration does not depend on the initial concentration. Consequently, the asymptotic form given in Eq. (2.15) is expected to hold for arbitrary random initial conditions.

Let us consider now the case where particles hop to a randomly chosen site, and annihilation occurs whenever an attempt to land on an occupied site is made. In this case, we ignore the spatial dimensionality, and we imagine that all sites are connected to each other. Thus, the concentration obeys the mean-field evolution equation $dc(t)/dt = -kc^2$, where k is the reaction rate, and whose solution is

$$c(t) = \frac{1}{c_0^{-1} + kt}. \tag{2.17}$$

At two dimensions, the block argument matches the mean-field behavior, and we conclude that critical dimension for this process is $d_c = 2$. Above this critical dimension, t^{-1} decay occurs. Furthermore, the slower than mean-field decay indicates an effective repulsion between particles. This repulsion is manifested by a vanishing interparticle distance distribution function [6]. This system is one example that illustrates the crucial role that spatial fluctuations play in low dimensions.

The block argument is a robust one; it remains the same for a class of microscopic interaction mechanism. For example, consider the coalescence process $A + A \to A$ [6], where the asymptotic form $(Dt)^{-1/2}$ should hold up to a prefactor. Indeed, the diffusion-limited fusion of photogenerated excitons in a one-dimensional tetramethylammonium manganese trichloride system was observed to obey this asymptotic decay [7].

As mentioned previously, the annihilating particles system is dual to an adsorption process. The mapping is simple; particles are identified with empty sites ("holes") and vice versa. Since a hop of a particle to the right, $AO \to OA$, is equivalent to a hop of a hole to the left, particle diffusion corresponds to hole diffusion. The annihilation process, on the other hand, $AA \to OO$, corresponds to adsorption of dimers. Hence, by reversing the time arrow, the annihilation process is mapped into the adsorption process. Therefore, the annihilation process is isomorphic to an adsorption process where pairs of particles adsorb on the surface with rate $2D$ and hop to nearest neighbor sites with rate D. In the adsorption process, the concentration, given by $1 - c(t)$, approaches unity with a power-law correction $t^{-1/2}$ [8]. In chapter 7, we discuss a closely related process occurring on the continuum where a logarithmic approach to the completely filled state occurs. It is also seen that irreversible adsorption, where particles are allowed to diffuse, is also isomorphic to the

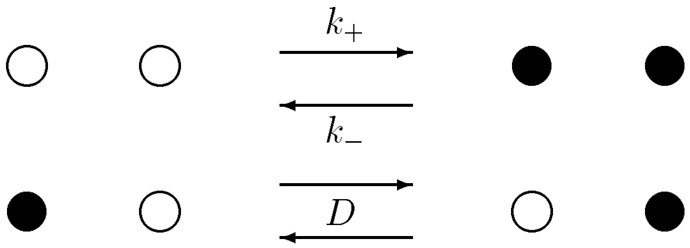

Figure 2.3: The reversible adsorption process

kinetic Ising model. In the next section, we expand this approach to one-dimensional adsorption-desorption processes.

2.3 Adsorption Processes: Role of Reversibility

In a reversible adsorption process, particles adsorb on a surface and similarly, particles are also allowed to desorb. Typically, the adsorbing particles are r-mers, *i. e.*, they occupy r consecutive lattice sites. In this section, we discuss an elementary dimer adsorption-desorption process. For an adsorption attempt to be successful, both sites must be vacant. The aforementioned mapping to the kinetic Ising model is used here to obtain the equilibrium solution and the asymptotic approach towards this state [9]. In the reversible adsorption case, dimers can adsorb only if both lattice site are vacant. The two adsorbing particles then diffuse independently on the surface, as shown in Figure 2.3. The three rates defining this process are the adsorption rate k_+, the desorption rate k_-, and the hopping rate D. Using the isomorphism to the spin model, established in the previous chapter (see figure 2.1), we match the above rates with the spin-flip rates $\alpha(1+\gamma)/2$, $\alpha(1-\gamma)/2$ and $\alpha/2$, respectively. Consequently, the temperature of the equivalent spin model is given by $\exp(-4J/k_BT) = k$, with $k = k_+/k_-$. Note that the kinetic Ising model has only two independent parameters and hence, the hopping rate cannot be arbitrary and is in fact given by $D = k_+ + k_-$. Using the pair correlation of Eq. (2.10) and Eq. (2.11), the equilibrium concentration is found to be

$$c^{eq}(k) = \frac{\sqrt{k}}{1+\sqrt{k}}. \tag{2.18}$$

For small adsorption rates, the concentration is an algebraic function of the normalized adsorption rate $c \sim \sqrt{k}$. In contrast, for reversible adsorption of monomers, the solution is a trivial one and the corresponding dependence is a linear one. The temporal approach to the equilibrium solution is related to the decay of the energy fluctuations in the Ising model, since r_1 is proportional to the average energy. The relaxation time τ is identical to the one previously found for the relaxation of the magnetization $\tau = 1/2(1-\gamma)$, and as a result,

$$\tau = \frac{1+k}{4k}. \tag{2.19}$$

The relaxation time diverges as k vanishes, reminiscent of a critical point.

However, the qualitative nature of this behavior changes drastically when the transition rules are changed. For example, when adsorption of monomers only is coupled with desorption of dimers, the following results were found, $c \sim k^{1/3}$ and $\tau \sim k^{-2/3}$ for $k \ll 1$. This result is obtained by noting that the monomer adsorption process corresponds to flipping all spins to the right of the adsorbing sites [9]. The two process are fundamentally different. While the former is reversible, the latter is not. Therefore, the steady state obtained in the monomer adsorption case is not an equilibrium one (detailed balance is not satisfied). Typically, most nonequilibrium process lead to a steady state that does not satisfy the detailed balance condition. This example illustrates that reversibility is a fundamental aspect of a stochastic process.

The desorption limited case sheds light on the importance of reversibility. While the concentration in the reversible case approaches unity for $k \to \infty$, non-trivial behavior occurs when adsorption only occurs, namely, irreversible adsorption. In this problem dimers are deposited randomly on an initially empty surface. An adsorption event is successful only if both sites are empty. With the empty initial conditions, the system reaches a jammed configuration, where no further adsorption events are possible. The steady-state density is given by the famous Flory result [10]

$$c_\infty = 1 - e^{-2}. \tag{2.20}$$

In appendix B, we detail a solution for the general for k-mer random sequential adsorption process in one-dimension, and Eq. (2.20) follows from the $k = 2$ solution. Starting from the partially occupied state with the dimers separated by a single vacant site, the initial state is left unchanged, and the density is always 2/3. This discrepancy shows that in the irreversible adsorption case the limiting concentration depends strongly on the initial conditions.

2.4 Fluctuation Dominated Reactions

In this section we solve for the concentration in a ballistic annihilation process [11]. The solution is then used to explain the significance of initial spatial fluctuations in determining the asymptotic kinetics. The similarity to diffusively-driven two-species annihilation is stressed using a heuristic argument.

The single-species ballistic annihilation process is defined as follows. Ballistic particles are distributed randomly with density c_0 on the continuum. Particles move with constant velocity, and a collision results in the annihilation of both colliding particles. Here we discuss the case where particles are assigned two opposite velocities: $+v_0$ with probability p_+, and similarly, $-v_0$ with probability $p_- = 1 - p_+$.

In the two-velocity case it is possible to identify all collision partners, given the initial positions of the particles. The collision times are then determined by incorporating the distances between the particles. Two particles can annihilate only if they are separated by an even number of particles. Denoting particles by their order, $k = 1, \ldots, 2n$, we define b_n as the probability that all such $2n$ particles eventually react among themselves, with $b_0 = 1$. For example, $b_1 = p_+p_-$. Taking into account all possible collision partners of the $k = 1$ particle gives a recursion relation for $n > 1$,

$$b_n = p_+p_- \sum_{k=0}^{n-1} b_k b_{n-1-k}. \tag{2.21}$$

By introducing the generating function $B(z) = \sum_{n=0} b_n z^n$ and summing Eq. (2.21) over all n, one finds

$$B(z) = \frac{1 - \sqrt{1 - 4p_+ p_- z}}{2p_+ p_- z}, \tag{2.22}$$

and by expanding $B(z)$ in a power-series one has

$$b_n = \frac{(p_+ p_-)^n (2n)!}{n!(n+1)!}. \tag{2.23}$$

Starting with an unequal concentration of right moving and left moving particles, the system reaches a state with the majority species only present, $c_\infty = c_0|p_+ - p_-|$. We now obtain the concentration for the uniform initial condition, where the separation between two neighboring particles is always $1/c_0$. To survive to time t, a particle has to avoid collisions with all k-particles such that $|k| > 2c_0 v_0 t$. Using the reaction probabilities, the time dependent concentration is written as $c(t) - c_\infty = 2c_0 p_+ p_- \sum_{n=[c_0 v_0 t]} b_n$. Substituting the actual reaction probability given by Eq. (2.23) in this expression yields the long time behavior of the concentration. When the initial concentration of the species are not equal, the concentration approaches the final state as $c(t) - c_\infty \sim (c_0 v_0 t)^{-3/2} \exp(-\text{const.} \cdot c_0 v_0 t)$. In contrast, when $p_- = p_+ = 1/2$, a power-law decay is found,

$$c(t) \sim \left(\frac{c_0}{2\pi v_0 t}\right)^{1/2}. \tag{2.24}$$

Despite the apparent similarity of the result with that of the diffusively-driven single-species annihilation, the underlying mechanism for the decay is different. While the corresponding $(Dt)^{-1/2}$ decay is independent of the initial conditions, the concentration of Eq. (2.24) exhibits a dependence on c_0.

A heuristic argument, similar to the one used describing the $A + A \to 0$ process, can be applied to determine the decay of the density in the ballistic case. We assume that within an interaction length l all $N = N_+ + N_-$ initially present particles have had a chance to interact. The total number of surviving particles will thus be $\Delta N = |N_+ - N_-|$. Using the central limit theorem, $\Delta N \sim \sqrt{N}$, and consequently, the asymptotic concentration is found

$$c \sim \frac{\sqrt{N}}{l} \sim \left(\frac{c_0}{l}\right)^{1/2}. \tag{2.25}$$

Substituting the interaction length $l \sim v_0 t$, the exact result of Eq. (2.24) is reproduced. It is seen that the system arranges into domains of particles moving with identical velocity. This spatial organization enhances the survival probability by a shielding mechanism. A right moving particle is protected from annihilation by all consecutive right moving particles placed to its right. Inspired in part by these initial spatial fluctuations effects, we consider in chapter 3 ballistic annihilation with continuous initial velocity distributions.

Another important process that exhibits strong dependence on initial fluctuations is the diffusively-driven two-species annihilation [12, 13, 14]. Here two different species, denoted by A and B, are randomly distributed initially with equal concentrations. Particles move diffusively, and reactions are allowed only between opposite species. The fluctuation argument, presented for the ballistic reaction case, is applicable here, and a generalization of Eq. (2.25) gives $c \sim (c_0/l)^{d/2}$. The interaction length grows according to $l \sim \sqrt{Dt}$ since the transport mechanism is diffusive. Consequently, the following asymptotic form of the concentration is found

$$c(t) \sim \left(\frac{c_0^2}{Dt}\right)^{d/4}. \tag{2.26}$$

The concentration crosses over to the mean-field behavior at $d_c = 4$. Again, the slower than mean-field behavior is made possible by formation of ever growing domains occupied by one species only.

All the soluble processes we presented in this chapter are deeply related to the theory of random walks. For example, b_n, the probability describing the ballistic annihilation process is identical to the probability that a biased random walker returns to its starting point for the first time at the n^{th} step. Furthermore, the concentration in the diffusive driven annihilation equals the probability that a continuous time random walk is at the origin at time t. Curiously, however, the transport mechanism in the ballistic reaction process is not a diffusive one.

Chapter 3

Non-Universal Decay Kinetics in Ballistic Annihilation

A number of interesting results have been recently reported for the kinetics of irreversible agglomeration. In an attempt to describe phenomena such as fluid vortices coalescence [15] and planet formation by accretion [16], the following idealized aggregation model has been introduced. In this process, written symbolically as $A_i + A_j \rightarrow A_{i+j}$, the trajectories are ballistic, and the collisions between aggregates conserve momentum [17, 18]. The subscripts i, j refer to the (conserved) mass of the aggregates. A scaling argument suggests that the concentration of aggregates decays as $t^{-\alpha}$, with $\alpha = 2d/(d+2)$, where d is the spatial dimension [17]. This dimension dependence for all d is atypical of the behavior pattern exhibited by diffusion-controlled reactions, as discussed in the review chapter. Moreover, we have shown in section 2.4 that the ballistic annihilation process $A + A \rightarrow 0$ with two opposite particle velocities exhibits anomalously slow decay kinetics. This behavior was accounted for by the formation of large-scale spatial heterogeneities, a mechanism similar to the one governing the diffusive-driven two-species annihilation [12, 14, 19, 20, 21]. This spatial organization enhances the survival probability of a single particle.

Motivated in part by these intriguing features, we investigate the decay kinetics of the elementary single-species annihilation process, $A + A \to 0$, for arbitrary continuous initial velocity distributions. Such processes describe actual nonequilibrium processes such as electron-hole recombination and the decay of excitations induced by irradiation [22, 23]. We find that the decay of the density strongly depends on the form of the initial velocity distribution. Moreover, faster particles annihilate at a higher rate, leading to a decay of the typical velocity as well.

We suggest a scaling argument, based on the typical collision time, that relates the concentration to the typical velocity. A Boltzmann equation for the evolution of the velocity distribution verifies this relation. Using the anticipated scaling forms of both the velocity and the velocity distribution, we eliminate the time variable from this equation. We combine the limiting behaviors of the velocity distribution into an ansatz solution. This solution suggests nonuniversal dependence of α, the exponent describing the concentration decay, on the details of the initial velocity distribution near the origin. In one and two dimensions, numerical integration of the Boltzmann equation and Monte Carlo simulations verify our predictions. The Boltzmann equation yields values of the decay exponents that are in good agreement with the actual simulations. We conclude that the success of this mean-field approximation is made possible by the relatively small velocity correlations between neighboring particles.

3.1 Scaling Properties

At time $t = 0$, the system consists of identical particles which are distributed in space with $P(v, t = 0)$ the initial concentration of particles of velocity v. For simplicity, only symmetric distributions with respect to the origin are studied. The decay kinetics appear to be independent of the initial spatial distribution of particles, and thus we focus on a random initial distribution of interparticle distances. Particles move according to their initial velocity until a collision occurs, which results in the removal of both colliding particles, as illustrated in Figure 3.1. We are interested in determining the time dependence of the macroscopic concentration, $c(t) = \int dv P(v, t)$, and the moments of the velocity distribution, $\langle v^n \rangle^{1/n} = \left(\int dv\, v^n P(v, t)/c(t)\right)^{1/n}$.

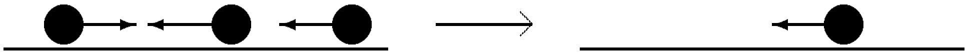

Figure 3.1: Illustration of the annihilation process

A simple power counting argument relates the exponents which characterize the decay of the concentration with the exponent corresponding to the typical velocity. Consider a system of identical particles of fixed radius r at concentration c which move with a velocity of the order of $v_{\rm rms}$. From an elementary mean-free path argument, the time between collisions is $t \sim 1/cv_{\rm rms}r^{d-1}$. If one assumes the following power law forms for the concentration and $v_{\rm rms}$,

$$c \sim t^{-\alpha} \qquad v_{\rm rms} \sim t^{-\beta}, \tag{3.1}$$

then the mean-free path argument indicates that the relation $\alpha + \beta = 1$ should hold for all spatial dimension d.

Since the lifetime of particles with velocity v is proportional to $1/v$, faster particles tend to annihilate more quickly, and the typical velocity should decay in time. By the relation between α and β, a value of α less than unity is therefore implied. We further argue that there is a strong dependence of the exponent α on the form of the initial velocity distribution. This behavior differs from the mean field prediction of $c \sim t^{-1}$ which arises from the naive rate equation $\dot{c} \propto -kc^2$.

3.2 The Boltzmann Equation

A useful approach for determining the decay kinetics is to write a Boltzmann equation for the time evolution of the velocity distribution. For simplicity, consider the case of one dimension; generalization to higher dimensions follows naturally. Let $P(x, v, t)$ be the density of particles with velocity v at position x and at time t. At time $t + \Delta t$, the velocity distribution changes both because of translation of particles and because of reactions. We treat the reaction term in a mean-field approximation by assuming that a particle at $x' < x$ and velocity $v' > v$ will necessarily react with the target particle at (x, v) when $x - x' < (v' - v)\Delta t$. There is a complementary contribution due to collisions between the target and a particle located at $x' > x$ with $v' < v$.

The sum of these two contributions leads to the Boltzmann equation for ballistic annihilation

$$\begin{aligned} &P(x + v\Delta t, v, t + \Delta t) - P(x, v, t) = \\ &-kP(x, v, t)\Big[\int\limits_{v}^{\infty} \int\limits_{x-(v'-v)\Delta t}^{x} dx'\, P(x', v', t) + \int\limits_{-\infty}^{v} dv' \int\limits_{x}^{x+(v-v')\Delta t} dx'\, P(x', v', t)\Big], \end{aligned} \tag{3.2}$$

where k is a dimensionless reaction constant. Since a collision leads to particle annihilation, there is no collision-induced gain term in the equation. This approximate equation overcounts collisions, since the incident particle at x' may react with a third particle rather than with the target particle.

To analyze the Boltzmann equation, we expand Eq. (3.2) to first order in Δt to arrive at

$$\frac{\partial P(x, v, t)}{\partial t} = -v\frac{\partial P(x, v, t)}{\partial x} - kP(x, v, t)\int\limits_{-\infty}^{\infty} dv' |v - v'| P(x, v', t)\,. \tag{3.3}$$

Since the initial velocity distribution is spatially homogeneous, and because of the homogeneity of the reaction process, we assume that the velocity distribution remains spatially homogeneous. Thus we write $P(v, t)$ to signify the time-dependent and spatially homogeneous density of particles with velocity v. This implies that the convective term $\partial P/\partial x$ in the Boltzmann equation may be set to zero, leading to

$$\frac{\partial P(v, t)}{\partial t} = -kP(v, t)\int\limits_{-\infty}^{\infty} dv'\, |v - v'| P(v', t)\,. \tag{3.4}$$

Thus the $|v - v'|$ dependence of the integral kernel controls the reaction rate between two particles. Eq. (3.4) is also strongly reminiscent of the Smoluchowski equation for ballistic aggregation [18]. Despite the uncontrolled nature of the approximations underlying Eq. (3.4), this formulation gives a useful quantitative description of the decay kinetics.

The first step in our analysis of the Boltzmann equation is to apply dimensional analysis, together with the assumed asymptotic behaviors, $c \sim t^{-\alpha}$ and $v_{\rm rms} \sim t^{-\beta}$, to reduce Eq. (3.4) to a single variable equation. From these considerations, we expect that the velocity distribution will have the following scaled form

$$P(v,t) = \frac{c_0}{v_0}\left(\frac{t}{t_0}\right)^{\beta-\alpha} f(z), \tag{3.5}$$

where the scaling function $f(z)$ depends only on the dimensionless velocity

$$z = \frac{v}{v_0}\left(\frac{t}{t_0}\right)^{\beta}. \tag{3.6}$$

Here $t_0 = 1/(kc_0v_0)$ is the initial characteristic time between reactions, with k the dimensionless reaction constant, c_0 the initial concentration, and v_0 the initial rms velocity.

Upon substituting this scaling form into Eq. (3.4), we confirm the anticipated exponent relation by equating all the resulting temporal prefactors

$$\alpha + \beta = 1. \tag{3.7}$$

Additionally, we obtain a rescaled Boltzmann equation for the scaling function

$$(2\beta - 1)f(z) + \beta z f'(z) = -f(z)\int_{-\infty}^{\infty} dz'\, |z - z'|\, f(z'). \tag{3.8}$$

Notice that this equation is invariant under the transformation $f(z) \to a^2 f(az)$, so that a unit normalization of $f(z)$ can be achieved by a scale change in z. We observe that the scaling form $f(z)$ depends heavily on the value of β, a behavior that was confirmed by direct numerical integration of the Boltzmann equation.

To find the tail of the scaled velocity distribution, we approximate $|z - z'| \sim |z|$ in the integral and use the fact that $f(z)$ vanishes as $z \to \infty$. These steps reduce Eq. (3.1) to a simple differential equation whose solution is

$$f(z) \sim |z|^{(1-2\beta)/\beta} \exp(-|z|/\beta), \qquad |z| \gg 1. \tag{3.9}$$

Near the origin, Eq. (3.8) admits different solutions for $f(z)$, and correspondingly, the exponent β depends on the form of the initial velocity distribution.

To treat the small-z limit, we first divide Eq. (3.8) by $f(z)$ to yield

$$(2\beta - 1) + \beta \lim_{z\to 0} z\,(\ln f(z))' = -2\int_0^\infty dz'\,|z'|\,f(z'). \tag{3.10}$$

Consider an initial velocity distribution with a power-law tail in the small velocity limit, $P(v,t=0) \propto |v|^\mu$. Our Monte Carlo simulations (discussed below) reveal that the scaled distribution retains the same power-law form, $f(z) \sim z^\mu$, in the small-z limit. By adopting this form in Eq. (3.10), the second term is simply equal to $\beta\mu$. The resulting equation then predicts that β is a monotonically decreasing function of μ (for $\mu > -1$) whose precise form depends on the first moment of $f(z)$. This moment, in turn, depends on the full details of the velocity distribution. For example, if we take as a trial function $f(z) \propto z^\mu e^{-z/\beta}$ in Eq. (3.10), *i. e.*, the product of the asymptotic behaviors, we obtain $\beta = 1/(3+2\mu)$. This estimated form qualitatively mirrors values for β obtained by numerical integration of Eq. (3.4) and on Monte Carlo simulations for various values of μ.

The generalization of the scaling approach for the Boltzmann equation to higher spatial dimensions is straightforward. The scaled velocity distribution function now takes the form

$$P(v,t) = \frac{c_0}{v_0}\left(\frac{t}{t_0}\right)^{\beta d-\alpha} f(\vec{z}\,), \quad \text{with} \quad \vec{z} = \frac{\vec{v}}{v_0}\left(\frac{t}{t_0}\right)^{\beta}, \tag{3.11}$$

where the exponent combination βd originates from an integration over d-dimensional velocity space. The corresponding rescaled equation for $f(\vec{z}\,)$ becomes

$$((d+1)\beta - 1)f(\vec{z}\,) + \beta\vec{z}\cdot\nabla f(\vec{z}\,) = -f(\vec{z}\,)\int\limits_{-\infty}^{\infty} d\vec{z}\,'|\vec{z} - \vec{z}\,'|f(\vec{z}\,'). \tag{3.12}$$

We emphasize that for higher dimensions, the Boltzmann equation involves a qualitatively different type of approximation in comparison with the one-dimensional case. To determine the relation between the exponents μ and β, we again assume a small-z power law form $f(\vec{z}\,) \propto |\vec{z}\,|^\mu$, with $\mu > -d$, and a relatively sharp cutoff in $f(\vec{z})$ for large $|\vec{z}\,|$. When employed in the Boltzmann equation, these assumptions again lead to a qualitatively correct μ-dependence of β. Namely, β monotonically decreases with μ, and has the limits $\beta \to 1$ for $\mu \to -d$ and $\beta \to 0$ for $\mu \to \infty$. As in the case of one dimension, if we adopt $f(\vec{z}) \propto |\vec{z}|^{\mu} e^{-|\vec{z}|/\beta}$, then Eq. (3.12) gives the $\beta = 1/(1 + 2d + 2\mu)$. Conversely, as the spatial dimension increases, β decreases systematically, and the limit $\alpha = 1$ is approached but never reached. This behavior corresponds to the naive rate equation $\dot{c} = -kc^2$. Thus only in the $d = \infty$ limit are particle trajectories sufficiently transparent that the typical velocity does not decrease. This is in contrast to the situation of many diffusion-controlled reactions for which "transparent" behavior occurs for only $d >= d_c$ with d_c finite [14].

3.3 Numerical Analysis

To test our approximate analysis, we have performed direct numerical integration of the Boltzmann equations, Eq. (3.4) and Eq. (3.12) (see Table 3.1). In one dimension, a typical integration was based on dividing the velocity range $[-1, 1]$ into 200 bins with a time step of $\Delta t = 0.15$. A finer level of resolution gives essentially identical results. The integration was performed to 1000 time steps. To estimate the value of β, we computed the "test" scaling function $f(z; t)_{\mathrm{test}} \propto t^{1-2\beta_{\mathrm{test}}} P(v, t)$ at different times and adjusted β_{test} to achieve the best data collapse between different data sets. By this method, we obtained estimates for the exponent β with an uncertainty of less than 0.005.

We also performed Monte Carlo simulations for ballistic annihilation in one and two dimensions which are based on two independent approaches. One method simulates the ballistic motion as a biased random walk. In two dimensions, a particle at $\vec{r}_i$ is assigned a velocity (v_{ix}, v_{ix}), with $|v_{ix}|, |v_{iy}| < 1$, according to an initial velocity distribution with support in $[-1, 1]^2$. A move attempt consists of picking each occupied site $\vec{r}_i$ at random, and the particle is moved by an amount $(\mathrm{sgn}(v_{ix}), 0)$ with probability $|v_{ix}|$ and by an amount $(0, \mathrm{sgn}(v_{iy}))$ with probability $|v_{iy}|$. If a particle lands on an occupied site, both particles are removed from the system. The time is then incremented by the inverse of the current number of particles in the system. The attraction of this stochastic method is that it is easily implemented

-bb-error = =

Figure 3.2: One-dimensional Monte Carlo simulation results for the concentration and the rms velocity *vs.* time. An average over 50 realizations on a 100000-site ring at initial concentration $c_0 = 0.5$. Shown are results for the "flat" initial distribution (empty symbols) and for the case $\mu = -1/2$ (filled symbols).

in any spatial dimension. However, the stochastic nature of the individual particle moves introduces diffusion in addition to the primary ballistic motion. This may lead to a crossover associated with the transition between diffusion and drift in a biased random walk. This feature can be overcome by carrying the simulation over a sufficiently large temporal range.

Our second method is an exact time evolution by synchronous dynamics, an approach which is practical to implement only in one spatial dimension. Particle velocities and positions are initialized on a periodic one-dimensional chain. The collision time for each nearest-neighbor pair is computed and the minimum pair collision time $\tau_{\rm min}$ is retained. The particles then move ballistically over a time $\tau_{\rm min}$, so that the particle pair whose collision time equals $\tau_{\rm min}$ is removed, and the time is incremented by $\tau_{\rm min}$. The determination of $\tau_{\rm min}$ and subsequent update of particle positions by this minimum time interval is then iterated.

Our two simulation methods give essentially identical results for continuous initial velocity distributions, and we quote exponent estimates based on the biased random walk algorithm, since it can be applied in both one and two dimensions (Table 3.1).

-bb-error = =

Figure 3.3: Monte Carlo simulation results for two-dimensions. An average over 500 realizations for a uniform distribution of velocities on a 100×100 lattice at initial concentration $c_0 = 0.3$.

The exponents are determined by measuring the slopes of successive pairs of data points when time-dependent quantities are plotted on a double logarithmic scale. Typically there is a non-negligible temporal range for which the value of the slope is most stable, and we adopt the average value of the slope in this range as the exponent estimate. The accuracy of the simulation can be inferred from the deviation of the numerical estimate for $\alpha + \beta$ from its expected value of unity.

The numerical integration of the Boltzmann equation provides an excellent approximation for the simulation results. The Boltzman equation overcounts reactions, and hence it provides an upper limit for the concentration decay exponent α (see Table 3.1). We also computed the velocity correlations between particles $r_k^2 = \langle v_i v_{i+k} \rangle / \langle v_i^2 \rangle$ resulting from the simulations. In the long time limit, this quantity reaches a constant, and we found $r_1 \cong 0.2$ and $r_2 \cong 0.05$, for the case $\mu = 0$. Hence, particles are only loosely correlated, thereby explaining the relative success of the decoupled Boltzmann equation.

		MC		NI
Dimension	μ	β	α	α
1	0	0.22	0.76	0.77
1	$-1/2$	0.42	0.56	0.60
1	$-4/5$	0.66	0.32	0.37
2	0	0.10	0.89	0.91

Table 3.1: Numerical values for the decay exponents α and β based on numerical integration (NI) of the Boltzmann equation, Eq. (3.4), and on Monte Carlo (MC) simulations. Results are given for several initial distributions. Note that $\alpha(\mathrm{NI}) > \alpha(\mathrm{MC})$.

3.4 Discussion

The non-universality displayed by ballistic single-species annihilation with continuous velocity distributions suggests several interesting avenues for further investigation. One such situation is ballistic annihilation with a trimodal initial velocity distribution, $P(v, t=0) \propto p_+\delta(v-1)+p_0\delta(v)+p_-\delta(v+1)$, with $p_++p_0+p_- = 1$. For the symmetric situation of $p_+ = p_-$, numerical simulations reveal interesting dependence on the sole parameter p_0 [24]. In the limit $p_0 \to 0$, the problem reduces to the bimodal case, and one finds $c_\pm \sim t^{-1/2}$ and $c_0 \sim t^{-1}$. The latter result follows from consideration of the survival probability of a stationary impurity in a background of right-moving and left-moving particles. Since such a single stationary particle has to avoids collisions from both sides, $c_0(t) \sim c_\pm(t)^2$, and the t^{-1} decay follows. We find that for $p_0 > p_c \cong 0.25$, a finite fraction of the stationary particles survives while the kinetic approach to this limit is exponential. At the transition point p_c, the density decays as a non-trivial power-law $t^{-2/3}$ for all three species. Below the transition point, the density obeys the behavior obtained in the vanishing p_0 limit. These intriguing features are yet to be understood analytically.

It may also prove interesting to study single species annihilation for which the diffusion coefficient of each reactant is drawn from a continuous distribution. Particles with a larger diffusion coefficient will explore a larger area and thus may be expected to decay more rapidly in time. Hence, it is reasonable to assume that the average diffusion coefficient of the surviving particles will decay according to the power law $\langle D\rangle \sim t^{-\beta}$. When this is used in an estimate of the mean collision time between particles, one finds the relation $2\alpha/d+\beta=1$ between the diffusion coefficient decay exponent and the concentration decay exponent. Based on the behavior observed in ballistic reactions, we anticipate that non-universality in α and β may also occur for reactions in which the particles possess continuously distributed diffusion coefficients. Recently, it was suggested that nongeneric decay occurs for $\mu < -1/2$ only, while the conventional decay of Eq. (2.15) occurs for $\mu > -1/2$ [25].

Another interesting variation is the ballistic aggregation, $A+A\to A$, in which the collision product takes on the velocity of one of the incident particles according to a specified rule. In the next chapter, we consider a situation where particles move with positive velocities and coalesce upon collisions. The motivation for this model comes from traffic flows in one-lane roads. This soluble process provides an analytical confirmation of our principal findings concerning the asymptotic behavior of the concentration and the velocity. Additionally, in chapter 5 we introduce superimposed diffusion to the bimodal velocity annihilation process. Unlike the continuous velocity distribution case, where diffusion was irrelevant to the outcome of the simulations, the kinetics in the two-velocity case is found to be sensitive to the addition of diffusion.

In summary, the kinetics of ballistic annihilation with general distributions of particle velocities exhibit a rich variety of asymptotic behavior. Both numerical and analytical approaches indicate that there is non-universality in the exponents that describe the time dependence of the concentration and the typical velocity. An approximate theory, based on a mean-field Boltzmann equation, successfully accounts for the dependence of these exponents on the initial velocity distribution. This success is accounted for by the "short memory" of the system, *i. e.*, the small velocity correlations between neighboring particles. As the spatial dimension is increased, the "transparent" limit $\alpha = 1$ is approached but apparently never reached.

Chapter 4

Ballistic Aggregation

Intrigued by the wide range of kinetics emerging from ballistic annihilation, we introduce a ballistically-controlled aggregation process. Furthermore, we are motivated by the growing number of attempts to describe collective properties of traffic flows by microscopic models which are controlled by ballistic transport and aggregation [26, 27]. For example, cellular automation models have been proposed to mimic congested traffic flow in two dimensions [28, 29]. Asymmetric hopping processes have also been applied to model traffic flow on a road [29, 30]. When the number of cars is large, traffic flows can be modeled in terms of a one-dimensional compressible gas [31, 32, 33]. Such an approach predicts the appearance of shock waves, where hydrodynamic quantities, such as the average density and velocity, become discontinuous. However, the hydrodynamic approach does not naturally describe the behavior of traffic flows where there are large heterogeneities in traffic density. The hydrodynamic approach is also based on phenomenological assumptions and uncontrolled mean-field like approximations.

In chapter 3, we discussed possible mechanisms for ballistic aggregation such as momentum conserving collisions and a selection rule with one of the colliding aggregates maintaining its velocity. In this chapter, we study the process schematically described by $A_{m_1,v_1} + A_{m_2,v_2} \to A_{m_1+m_2,\min\{v_1,v_2\}}$. We denote by $A_{m,v}$ a mass m cluster moving with velocity v. In other words, particles move ballistically in a single direction, say to the right, and clusters form whenever a faster particle overtakes a slower particle or cluster. Each cluster moves at the velocity of the slowest particle at the head of the cluster. This model is an idealization of a one-lane traffic flow. However, the appealing simplicity of the model suggests that it may be applicable to other clustering phenomena. Additionally, the model is soluble and permits a thorough understanding of the kinetics of the aggregation process.

We first present the model and investigate the scaling behavior of the velocity and the concentration of the clusters. Since the velocity of the slowest particle characterizes the velocity of an aggregate, we make use of the statistical properties of the minimal random variable within a large sample. It is found that both the concentration and the typical velocity obey asymptotic decays, which are similar to the ballistic annihilation process. To analyze the velocity distribution, the cluster mass is irrelevant, and hence, the derived "coalescence only" model needs to be considered. The velocity distribution is obtained exactly in terms of the initial distribution of particle velocities and evaluated for general continuous distributions. Furthermore, the velocity distribution obeys an exact Boltzmann equation reminiscent of the Boltzmann equation for the ballistic annihilation process of chapter 3. The general clustering process is then solved, and an asymptotically exact expression for the joint cluster mass-velocity distribution is obtained. In addition, formal solutions are presented for a generalization to situations in which there is a spatially and temporally homogeneous input of particles. In this case, the scaling analysis of the exact solution indicates two regimes of behavior. Depending on the functional form of the input velocity distribution, the resulting traffic distribution either continues to evolve with an ever-growing density or reaches a steady state.

4.1 Scaling Analysis

Initially, the system consists of identical point-like particles distributed randomly in space with a concentration c_0. We consider the initial velocity distribution,

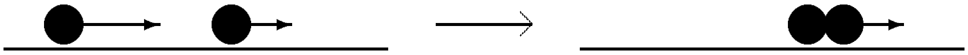

Figure 4.1: The aggregation process. A faster particle overtakes a slower particle and after the encounter, the faster particle assumes the velocity of the slower particle.

$P(v,t=0)$, which can generally be written in the scaling form

$$P(v,t=0) = \frac{c_0}{v_0} P_0\left(\frac{v}{v_0}\right) \qquad v > 0, \tag{4.1}$$

with $\int_0^\infty P_0(z)dz = 1$. Here we have tacitly subtracted the assumed finite value of the velocity of the slowest particle from all velocities. In addition, it is convenient to introduce the dimensionless density $c/c_0 \to c$, velocity $v/v_0 \to v$ and time $c_0 v_0 t \to t$. This yields a rescaled initial concentration which is equal to unity.

In this model, particles move with their initial velocities and aggregate upon collision. The aggregation rule is simple: two colliding clusters form a new cluster with a velocity equal to the smaller of the two incident cluster velocities and with a mass equal to the sum of the two cluster masses (see Figure 1). Denoting a cluster of mass m and velocity v by $A_{m,v}$, the process is described by the reaction scheme

$$A_{m_1,v_1} + A_{m_2,v_2} \to A_{m_1+m_2,\min\{v_1,v_2\}}. \tag{4.2}$$

We present now a simple argument, based on the statistics of extremes, to predict the asymptotic time dependence of the mass and the velocity. Let m and v be the typical cluster mass and cluster velocity at time t. Thus, the typical distance, l, between clusters grows with time as $l \sim vt$. Since the typical number of particles in a cluster is proportional to the typical distance between clusters, one has $m \sim l \sim vt$. To find the typical velocity, one has to formulate a relation between the mass of a cluster and its velocity. Such a relation may be found exactly for an auxiliary "one-sided" problem in which particles are placed to the left of a given particle, and no particles are placed to the right. Eventually, this particle moving with velocity v will form a cluster that includes all consecutive particles to its left whose initial velocities are larger than v. The probability that there are exactly k such particles is equal to $P_- P_+^k$, with $P_+(v)$ ($P_-(v)$) defined as the probability that a particle has a velocity larger (smaller) than v, *i. e.*, $P_+(v) = \int_v^\infty P_0(v')dv'$. Therefore, the average number of particles in the cluster that ultimately forms is given by

$$\langle n(v)\rangle = \sum_1^\infty kP_-P_+^k = P_+/P_-. \tag{4.3}$$

Let us now assume a power-law behavior of the initial velocity distribution for small velocities,

$$P_0(v) \simeq av^\mu, \qquad v \ll 1 \tag{4.4}$$

with $\mu > -1$ for normalizability. Imposing this power-law form in Eq. (4.3) yields

$$\langle n(v)\rangle = \frac{P_+(v)}{P_-(v)} \propto \frac{1}{v^{\mu+1}}, \tag{4.5}$$

for sufficiently low velocities. For a particle moving with the typical velocity, it is reasonable to expect that this result, derived for the "one-sided" problem, gives a correct estimate for the original "two-sided" problem. Combining Eq. (4.5) with our previous estimate $m \sim vt$ yields the following asymptotic relations,

$$\begin{aligned} n &\sim t^\alpha \quad \text{with} \quad \alpha = \tfrac{\mu+1}{\mu+2}, \\ v &\sim t^{-\beta} \quad \text{with} \quad \beta = \tfrac{1}{\mu+2} \end{aligned} \tag{4.6}$$

Since the mass, or equivalently, the number of particles in a cluster, is conserved in the aggregation process, $cm \sim$ const. Therefore, the concentration of clusters, $c(t)$, decays as $c \sim t^{-\alpha}$. Notice that in the limit $\mu \to \infty$, the mass grows linearly with time. In contrast, when $\mu \to -1$, the mass is roughly constant, since the velocity distribution becomes effectively unimodal and collisions are absent. This qualitative dependence on the form of the initial velocity distribution is reminiscent of the ballistic annihilation process discussed in chapter 3. In both processes, one finds that the fundamental exponents are related by, $\alpha + \beta = 1$, which is merely a consequence of the relation $c \sim 1/vt$. Moreover, the decay exponents have similar functional dependences on the form of the initial velocity distribution for the two processes. However, the values of the decay exponents are different: for the "flat distribution" (corresponding to $\mu = 0$) one finds $\alpha = 1/2$ for the traffic model, while $\alpha \cong 0.76$ emerges from simulations of the annihilation process (see Table 3.1). Despite the qualitative similarity between these two models for continuous velocity distributions, different behaviors occur for discrete distributions. For such distributions, the concentration decays algebraically in time for ballistic annihilation, while the concentration decays exponentially in time for the traffic model.

Since both the mean mass and the velocity scale as power laws in time, the probability of finding a cluster of mass m and velocity v, $P_m(v,t)$, is expected to evolve toward a scaling distribution. Taking into account mass conservation, $\int dv \sum_n nP_m(v,t) = \text{const.}$, we postulate the scaling form

$$P_m(v,t) \simeq t^{\beta-2\alpha}\Phi(M,V), \tag{4.7}$$

for the joint distribution. The scaled mass, M, and scaled velocity, V, are defined by

$$M = m/t^{\alpha} \qquad \text{and} \qquad V = vt^{\beta}. \tag{4.8}$$

While the mass m is a discrete variable, the rescaled mass M is continuous. Once the joint mass-velocity distribution is found, the single variable mass and velocity distributions can be found by suitable integrations over the subsidiary variable.

Thus the velocity distribution, $P(v,t) = \sum_n P_m(v,t)$, should have the scaling form

$$P(v,t) \simeq t^{\beta-\alpha}\Phi_v(V), \tag{4.9}$$

with $\Phi_v(V) = \int_0^\infty dM\Phi(M,V)$, while the cluster-mass distribution, $P_m(t) = \int dvP_m(v,t)$, should have the scaling form

$$P_m(t) \simeq t^{-2\alpha}\Phi_m(M), \tag{4.10}$$

with $\Phi_m(M) = \int_0^\infty dV\Phi(M,V)$.

4.2 The Survival Probability

As a preliminary step in obtaining a full solution for traffic clustering, we derive the velocity distribution function $P(v,t)$. For studying the latter quantity, we can ignore the mass and focus only on the survival probability of a given particle. The evolution of this distribution is governed by the "derived" coalescence process

$$A_{v_1} + A_{v_2} \to A_{\min\{v_1,v_2\}}. \tag{4.11}$$

Notice that the density of particles with velocity v in the coalescence process is identical to $P(v,t)$, the velocity distribution of clusters in the full traffic aggregation model, Eq. (4.2).

Let $S(v,t)$ be the survival probability of particles of velocity v at time t. Here "survival" means a particle does not overtake any traffic, but an overtaken particle is still defined as surviving. Then the velocity distribution function is given by

$$P(v,t) = P_0(v)S(v,t). \tag{4.12}$$

The survival probability $S(v,t)$ can be found by considering the possible collisions of a particle with initial velocity v and initial position x with slower particles initially placed to its right. A collision with a slower v'-particle does not occur up to time t if the interval $[x, x+(v-v')t]$ does not include this particle. For an initial velocity distribution, $P_0(v)$, and a Poissonian initial spatial distribution, the probability that a particle with velocity between v' and $v'+dv'$ is absent in the interval $[x, x+(v-v')t]$ equals

$$\exp\left[-dv' P_0(v')(v-v')t\right]. \tag{4.13}$$

Now we argue that for a particle to survive to time t, the exclusion probability described in Eq. (4.13) should be taken into account for every $v' < v$. Let us assume otherwise and derive a contradiction. Consider a particle with initial position and velocity x and v respectively that has maintained its original velocity to time t. In addition, assume a slower v'-particle was initially present at the above exclusion zone, *i. e.*, $\Delta x(0) < \Delta v(0)t$. Here $\Delta x(t)$ is the distance between the two particles and $\Delta v(t)$ the relative velocity at time t. Since the velocity v' can only be lowered over time due to collisions, one has $\Delta v(t) \geq \Delta v(0)$. Consequently, at time t, the separation between the two particles, $\Delta x(t) = \Delta x(0) - \int_0^t \Delta v(t')dt' \leq \Delta x(0) - \Delta v(0)t < 0$, is negative in contradiction with the assumption that the v-particle survived. Hence, the survival probability is simply a product of the exponential factors of Eq. (4.13) for all v', with $v' < v$. Evaluating this product gives the survival probability

$$S(v,t) = \exp\left[-t\int_0^v dv'(v-v')P_0(v')\right]. \tag{4.14}$$

Combining Eqs. (4.12) and Eq. (4.14) yields the velocity distribution,

$$P(v,t) = P_0(v)\exp\left[-t\int_0^v dv'(v-v')P_0(v')\right], \tag{4.15}$$

which is valid for an *arbitrary* initial velocity distribution $P_0(v)$. The sole stochastic nature of the process arises from the initial conditions. For discrete initial distributions we see from Eq. (4.15) that the approach to the final concentration is exponential in time. Thus, we focus only on continuous initial distributions.

The velocity distribution can be readily calculated for the power-law initial velocity distribution of Eq. (4.4). In the long-time limit, the distribution function reaches a form that is independent of the details of the large-velocity tail of the initial distribution,

$$P(v,t) \simeq av^{\mu}\exp\left[-btv^{\mu+2}\right]. \tag{4.16}$$

with a and μ defined in Eq. (4.4) and $b = a/(\mu+1)(\mu+2)$. This expression can be written in the scaling form of Eq. (4.9) with the scaling function

$$\Phi_v(V) = aV^{\mu}\exp\left[-bV^{\mu+2}\right]. \tag{4.17}$$

From this exact solution one can see that the velocity distribution maintains its original power-law form for sufficiently small velocities. The exact solution validates the scaling assumption that the asymptotic decay and the shape of the limiting distribution are entirely determined by the low-velocity part of the initial distribution which, in turn, is governed by the exponent μ.

From Eq. (4.16), the total concentration, $c(t) = \int_0^\infty dv\, P(v,t)$, is

$$c(t) \simeq a(\mu+1)\Gamma(\alpha)(bt)^{-\alpha}. \tag{4.18}$$

Similarly, the average cluster velocity, $\langle v(t)\rangle = \int dv\, vP(v,t)/\int dvP(v,t)$, is

$$\langle v(t)\rangle \simeq \frac{1}{\Gamma(\alpha)}(bt)^{-\beta}. \tag{4.19}$$

The above expressions confirm the scaling laws suggested in Eq. (4.6).

Interestingly, the exact solution of Eq. (4.15) satisfies the following Boltzmann-like integro-differential equation,

$$\frac{\partial P(v,t)}{\partial t} = -P(v,t)\int_0^v dv'(v-v')P(v',0). \tag{4.20}$$

This equation suggests that the loss of v-particles due to collisions with slower v'-particles occurs at a rate proportional to the relative velocity, $(v-v')$. Moreover, the pair correlation function factorizes into a product of single-particle velocity distributions, $P(v,v',t) = P(v,t)P(v',0)$. Notice that in this decomposition, however, the distribution function for the smaller velocity, v', is evaluated at $t=0$, while in the Boltzmann equation of Eq. (3.4) the decomposition would involve the same argument for each velocity distribution. We postulate that a similar "effective time" type of equation might hold for the annihilation model. In addition, the exact Eq. (4.20) quantitatively demonstrates the degree of approximation of the mean-field Boltzmann equation.

The approach given above can be generalized in a straightforward way for the case in whihc the initial velocity distribution, $P_0(x,v)$, is spatially heterogeneous. The resulting time dependent velocity distribution, $P(x,v,t)$, turns out to retain this same spatial dependence. The solution is a generalization of Eq. (4.15),

$$P(x,v,t) = P_0(x-vt,v)\exp\left[-t\int_0^v dv'\int_{x-vt}^{x-v't} dx' P_0(x',v')\right], \tag{4.21}$$

where we have transformed to a coordinate system which moves with velocity v. Interestingly, imposing a step function as the initial spatial distribution leads to a logarithmically growing number of particles in the initially empty region [34]. It might also prove insightful to subject the above solution to other nontrivial initial spatial distributions.

4.3 The Full Probability Distribution

We now present a solution for the joint mass-velocity distribution function for the general traffic model. To obtain $P_m(v,t)$, the density of clusters of mass m

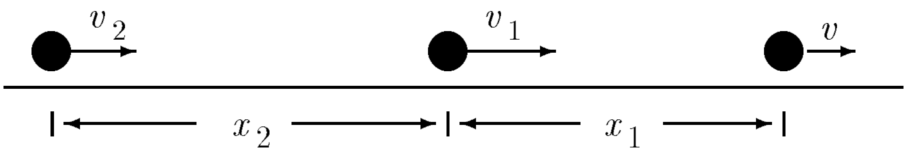

Figure 4.2: Illustration of the initial configuration of a possible three particle cluster.

and velocity v, it is useful to introduce the cumulative distribution, $Q_m(v,t)$, the distribution of clusters of velocity v and mass greater than or equal to m. Once the latter distribution is known, $P_m(v,t)$ can be obtained by

$$P_m(v,t) = Q_m(v,t) - Q_{m+1}(v,t). \tag{4.22}$$

Notice that the density of clusters of mass greater or equal to one is equal to the total cluster density, $Q_1(v,t) = P(v,t)$.

Consider a cluster of velocity v which contains at least m particles. Let us number the consecutive particles in a cluster from right to left by the index i and denote the rightmost particle as $i = 0$. Denote the initial distance between the i^{th} particle and the $(i-1)^{\text{th}}$ particle as x_i, as illustrated in Figure (4.2). We first solve for $Q_2(v,t)$ and then generalize the result for any m. Since $Q_2(v,t)$ is the probability that a cluster of velocity v has at least two particles at time t, it is equal to the product of the probability that the particle $i = 0$ has survived up to time t, $P(v,t)$, and the probability that the cluster $i = 1$ (whose mass may be larger than unity) collides with the particle $i = 0$ prior to time t. To calculate this collision probability we note that it is necessary that the collision partner from the left ($i = 1$) has a velocity larger than v and that the distance x_1 is smaller than $(v_1 - v)t$. Since the initial density of particles of velocity v_1 is $P_0(v_1)$, while the probability that an interval of length x_1 is empty is $\exp(-x_1)$, the joint velocity-distance density function for the particle $i = 1$ is the product, $P_0(v_1)\exp(-x_1)$. Integration of this density over velocities larger than v and over the proper distance interval gives the collision probability

$$Q_2(t) = P(v,t)\int_v^\infty dv_1 P_0(v_1) \int\limits_{x_1<(v_1-v)t} dx_1 \exp(-x_1). \tag{4.23}$$

The fact that the next to right particle cannot be slowed down by any other particle before colliding with the v particle is crucial in obtaining the solution.

To derive the general expression for $Q_m(v,t)$, the same joint velocity distance distribution $P_0(v_i)\exp(-x_i)$ is integrated over the position and velocity of the i^{th} particle for $i = 1, \ldots, m-1$. To ensure a collision, all $m-1$ particles have to move faster than the lead particle, and the distance of the i^{th} particle from the lead particle must obey $x_1 + \cdots + x_i \leq (v_i - v)t$. Imposing these constraints upon the integration over the velocity and distance of the $m-1$ additional particles yields the formal exact expression for the cumulative mass-velocity distribution,

$$Q_m(v,t) = P(v,t) \prod_{i=1}^{m-1} \int_v^\infty dv_i P_0(v_i) \int\limits_{x_1+\cdots+x_i<(v_i-v)t} dx_i \exp(-x_i). \tag{4.24}$$

For the case where the initial velocity distribution has the small velocity power-law tail of Eq. (4.4), we find the following asymptotic behavior

$$Q_m(v,t) \simeq t^{\beta-\alpha} a V^\mu \exp\left[-b(V+M)^{\mu+2}\right], \tag{4.25}$$

in terms of the scaling variables $M = m/t^\alpha$ and $V = vt^\beta$. A derivation of Eq. (4.25) is given in Appendix C.

In the long time limit, the joint cluster-mass distribution, $P_m(v,t) = Q_m(v,t) - Q_{m+1}(v,t)$ can be approximated by $P_m = Q_m - Q_{m+1} \to -\partial Q_m/\partial m$. Performing the differentiation gives the asymptotic form of the joint distribution,

$$P_m(v,t) \simeq t^{\beta-2\alpha} ab(\mu+2) V^\mu (V+M)^{\mu+1} \exp\left[-b(V+M)^{\mu+2}\right], \tag{4.26}$$

which has been explicitly written in the scaling form of Eq. (4.7). For arbitrary μ we are not able to evaluate the integral over the velocity to obtain the mass distribution explicitly. However, for the particular case of the flat distribution, $\mu = 0$, the integration is simple, and we find

$$\Phi_m(M) = a \exp(-aM^2/2) \qquad \mu = 0. \tag{4.27}$$

An amusing feature of the joint distribution function $\Phi(M,V)$ in the case $\mu = 0$ is the symmetry with respect to the variables V and M. Thus the cluster mass distribution, Φ_m, and the cluster velocity distribution, Φ_v, are identical Gaussian functions.

4.4 Clustering in Traffic Flow with Input

In this section, we investigate the evolution of traffic clustering in a generalization where there is a spatially uniform flux of particles. This is motivated by the fact that in real traffic situations the system is not closed; particles may enter and exit a roadway. For simplicity, we consider the case of a spatially homogeneous input of particles. A formal solution for the velocity distribution function can be obtained using techniques similar to those employed for the traffic coalescence model with no input.

We denote the input rate of particles (per unit length) with velocity v at time t as $R(v,t)$. The velocity distribution function for this system, $P(v,t)$, can be expressed as a convolution of the flux and the survival probability of a particle in the presence of the input, $S_I(v,t,t')$,

$$P(v,t) = \int_0^t dt'\, R(v,t')\, S_I(v,t,t'). \tag{4.28}$$

In writing this expression, we are assuming that the system is initially empty. The quantity $S_I(v,t,t')$ is the probability that a particle which is injected at time t' maintains its velocity to time t in the presence of the input. For such a particle to survive until time t, it has to avoid collisions with all slower particles which were present in the system at time t', as well as avoid collisions with all particles which are injected at later times t'', with $t > t'' > t'$. The probability for this composite event is simply the product of the probabilities of each event, and is given by

$$S_I(v,t,t') = \exp\left[-\int_0^v (v-v')dv' \left\{P(v',t')(t-t') + \int_{t'}^t dt'' R(v',t'')(t-t'')\right\}\right]. \tag{4.29}$$

The first factor, obtained from Eq. (4.14) by replacing $P_0(v')$ with $P(v',t')$, represents the probability of avoiding a collision with particles injected prior to time t'. The second factor represents the product of exclusions of the type written in Eq. (4.14) for times larger than t' and velocities smaller than v'. This factor accounts for the probability that there are no collisions with particles injected at times later than t'. Note that the kernel of the second factor involves the input rate R at time t'', which plays the role of the initial velocity distribution at this instant of time.

Eqs. (4.28) and (4.29) represent a formal solution to the kinetics of traffic clustering in the presence of homogeneous input of particles. For concreteness in determining how the input influences the asymptotic behavior of the cluster distributions, consider the case of a constant flux in time and space, $R(v,t) = hP_0(v)$, with $\int dv P_0(v) = 1$. By evaluating the velocity distribution under these conditions, one obtains the integral equation

$$P(v,t) = hP_0(v)\int_0^t dt' \exp\left[\int_0^v dv'(v-v')(t-t')\Big\{P(v',t') - hP_0(v)(t-t')/2\Big\}\right]. \tag{4.30}$$

Motivated by the nature of the results in the case of no input, consider again a power-law initial velocity distribution, $P_0(v) \sim v^\mu$, for small velocities. Let us assume power-law asymptotic behavior for the concentration, $c \sim t^{-\alpha}$, and the velocity, $v \sim t^{-\beta}$, as well as for the scaling form of Eq. (4.9) for the velocity distribution, $P(v,t) \sim t^{\beta-\alpha}\Phi_v(V)$. In addition, the only relevant part of the velocity distribution asymptotically is the small velocity limit where, $P(v,t) \sim v^\mu \sim t^{-\beta\mu}$. We now substitute the suggested scaling form into Eq. (4.30) and use power counting to extract the relations satisfied by the exponents α and β. For example, the powers of time on the left hand side and the right hand side of Eq. (4.30) should be equal, and consequently, $\beta(\mu+1) - \alpha = 1$. Neither term in the exponent should depend on time explicitly, leading to the familiar relation $\alpha + \beta = 1$. Solving for the decay exponents yields $\alpha = \mu/(\mu+2)$ and $\beta = 2/(\mu+2)$. Interestingly, these scaling relations predict a decaying cluster concentration, in the case of positive μ, in contradiction with the constant flux formulation of the problem. Thus, we conclude that the above scaling behavior holds for $\mu < 0$. On the other hand, for positive μ the system reaches a steady state with a constant concentration and a typical cluster mass $m \sim t$. At the transition $\mu = 0$ logarithmic temporal dependence might occur. The form of the steady-state density can be obtained by further analysis of the formal solution.

4.5 Discussion

In this chapter, we introduced a simple model that mimics the kinetics of clustering in a single lane of traffic. Through a direct probabilistic approach, the analytical forms of the cluster velocity distribution and the joint mass-velocity distribution have been derived. For an initial velocity distribution with a power-law behavior in the small velocity limit, both the average velocity and the average mass of aggregates exhibit an algebraic dependence on time. This asymptotic behavior depends directly on the nature of the initial velocity distribution of the slow particles. The qualitative asymptotic behavior is similar to that observed in the closely related ballistic annihilation, presented in chapter 3. We also investigated the evolution of an initially empty system with a steady input of particles. We found that this system exhibits a transition to a steady state for $\mu > 0$, while for $\mu < 0$ the system evolves to a scaling form with both the concentration and the velocity exhibiting an algebraic temporal behavior.

For the annihilation process, small correlations were responsible for the somewhat unexpected success of the mean-field approach. Thus, it may also be insightful to obtain analytically the same property in the aggregation process. Since clusters that move with velocity similar to that of their neighbors survive for longer times, we postulate that velocity correlations are indeed present in the system. The correlation length, associated with the decay of the velocity correlations, can be used to characterize possible spatial organizations.

The aggregation model introduced in this paper is irreversible and leads to a situation with ever-growing clusters. To describe traffic flows more realistically, several mechanisms to induce a steady state can be envisioned. For example, the input model can be generalized to incorporate a flux out of the system. Another realistic direction is to allow a faster particle to pass a slower particle at a rate which is some function of the velocity difference of the two particles. This would allow a fast particle to traverse a cluster particle-by-particle and ultimately regain its intrinsic velocity once the cluster is completely passed in analogy with real traffic flows.

Chapter 5

Asynchronous Ballistic Annihilation

In chapter 3, two techniques were applied to simulate ballistic annihilation. The first mimics the transport process using biased random walks, while the second simulates the purely ballistic motion. Modeling ballistic motion by biased random walks is equivalent to introducing diffusion. A naive argument suggests that diffusion is subdominant for sufficiently large times, and hence both methods are equivalent. This expectation was confirmed by the fact that the results for continuous velocity distributions were indistinguishable. However, for the bimodal-velocity distribution case, presented in chapter 2, we discovered that the outcome was strongly dependent on the technique we used.

In this chapter, we discuss the effect of diffusion on the bimodal velocity annihilation process and suggest a scaling argument which predicts that the model belongs to a new universality class. This argument is based on matching an ansatz for the decay of the concentration in the general situation to the corresponding expressions for the cases of a vanishing diffusion constant and a vanishing velocity. Both forms were rederived analytically in chapter 2. In analogy with the real-space renormalization argument used to explain the asymptotic kinetics in these limiting cases, we suggest that the system organizes according to two length scales. The smaller length scale characterizes the diffusion-controlled regime, *i. e.*, the spatial extent over which the identity of the particle is irrelevant. On the other hand, the annihilation process proceeds over the larger length scale as if diffusion were absent. Our numerical simulations provide evidence in favor of the predicted decay of the concentration. However, so far we were unable to find a sound theory that describes this interesting behavior.

In view of the lack of theoretical analysis, we also study this process by means of time power series techniques. We take advantage of the biased random walk simulation approach and represent this process by a sequential stochastic process. We model diffusion by requiring that particles move serially. This approach allows us to write linear rate equations for the microscopic configurations of the system. We then study the time evolution of the concentration by exact enumeration of all states of the system for short times. We suggest a Padé analysis for estimating the asymptotic properties of the emerging time power-series. To test this analysis technique, we use the solution to the diffusive $A + A \to 0$ model presented in the review. For the asynchronous ballistic annihilation case we evaluate numerically the first 17 terms in the time-series expansion of the concentration. Finally, we apply the suggested analysis mechanism to this series and find reasonable agreement with the scaling argument and the simulations.

5.1 Scaling Analysis

Consider a ballistic annihilation process in one dimension in which each particle moves ballistically with velocity v_0 or $-v_0$ with equal probabilities. If particles move one at a time, *i.e.*, asynchronous dynamics, there is diffusion in addition to the primary ballistic motion. A simple calculation shows that this procedure gives rise to a constant diffusion coefficient. This diffusive transport component permits two particles with the same velocity to annihilate. We present a scaling argument which suggests that the decay exponent α should equal 3/4 and perform Monte-Carlo simulations that support this argument.

The asynchronous ballistic annihilation process is completely characterized by three basic parameters, the velocity v_0, the diffusion constant D and the initial concentration c_0. This representation is useful since exact solutions are known for the two limiting cases, $D = 0$ and $v_0 = 0$, and these can be incorporated to produce the general case result. Using the three basic length scales $1/c_0$, $\sqrt{Dt}$ and $v_0 t$, we first write the most general ansatz for the concentration for $D, v_0 \neq 0$. Then we match it to the known limiting solutions for the two limiting cases, $D = 0$ and $v_0 = 0$, at the respective crossover times between the general behavior and the limiting behavior. The concentration in the general case must have the form

$$c(t) = c_0^{\beta} \left(\frac{1}{v_0 t}\right)^{\gamma} \left(\frac{1}{\sqrt{Dt}}\right)^{\delta}, \tag{5.1}$$

that is, $c(t)$ is a geometric average of the fundamental concentrations c_0, $1/v_0 t$ and $1/\sqrt{Dt}$. To ensure the proper dimensions of $c(t)$, the exponents β, γ and δ must obey the constraint $\beta + \gamma + \delta = 1$. In the case of a small drift [4, 5], the exact asymptotic form of the concentration for $v_0 = 0$, $c_D(t) \sim (Dt)^{-1/2}$ holds for $\sqrt{Dt} > v_0 t$ and matches Eq. (5.1) at the crossover time $t_1 = D/v^2$. Note that the crossover time is independent of the initial concentration, since the asymptotic kinetics of the diffusive process are universal, as discussed in chapter 2. Imposing $c_D(t_1) = c(t_1)$ and equating corresponding powers of the various coefficients yield the equation $\gamma + \delta = 1$. In the same way, the exact drift-limited solution [11] $c_v(t) \sim (c_0/v_0 t)^{1/2}$ should coincide with Eq. (5.1) at $t_2 = 1/Dc_0^2$. This condition leads to $\gamma = 1/2$. Consequently, $c(t)$ has the general form

$$c(t) \sim \left(\frac{1}{Dv_0^2 t^3}\right)^{1/4}. \tag{5.2}$$

Interestingly, the decay of the concentration in the general case is faster than that of the two limiting cases of $v_0 = 0$ and $D = 0$. Moreover, although one can claim that the diffusive nature of the particles does not play a role for sufficiently large times, this scaling argument suggests otherwise. Following the discussion in section 2.2, we expect that at time t, there exist a diffusive interaction length l_D,

-bb-error = =

Figure 5.1: Decay of the concentration(dots) from Monte-Carlo simulation. A line of slope $-3/4$ is shown for reference.

over which the diffusive transport dominates and particles are effectively identical. Once all particles interact inside such a box, only a single particle typically survives, and consequently, the concentration of the surviving ballistic particles is $c_{\pm} \sim 1/l_D$. There also exists a ballistic interaction length, l_v, that characterizes the interaction between opposite velocity particles. Inside such a box, fluctuations in the number difference dominate the process, and eventually only the majority species survives. Using the portion of particles that survive the diffusive-driven reaction as an effective concentration, we have $\sqrt{c_{\pm}/l_v}$, as obtained in chapter 2.4. Combining the two estimates yields $c \sim (1/l_d l_v)^{1/2}$. By substituting the temporal dependence of the interaction lengths $l_D \sim \sqrt{Dt}$ and $l_v \sim v_0 t$, we recover Eq. (5.2). Of course, both arguments we presented are identical, since they are based on the assumption that the ballistic+diffusive reaction can be decomposed into two independent mechanisms on different time scales or equivalently, length scales.

We have performed a Monte-Carlo simulation to verify these predictions. Initially the system consists of positive moving particles and negative moving particles distributed with equal probability. A simulation step consists of choosing a particle at random and moving it one lattice site. A positive particle is always moved to the right and similarly for a negative one. An attempt to land on an occupied site results in the removal of both particles from the system. Time is updated after each simulation step by the inverse number of particles. The results shown in Figure 5.1 correspond to an average over 10 realizations of 10000 particles. Since all relevant parameters have been taken of the order of unity, no early $t^{-1/2}$ decay is seen. The simulation provides additional evidence supporting the above $t^{-3/4}$ asymptotic decay of the concentration.

5.2 Time Series Studies

The sequential nature of the process suggests the representation of the concentration by a power-series in time as an avenue for numerical investigation. In the following we develop a formalism, which is applicable to general reaction schemes and use it to study asynchronous ballistic annihilation. In the case of sequential processes, one is naturally led to use representation number formalism, from which a linear rate equation emerge [35, 36]. From a theoretical viewpoint, exact methods [4] as well as renormalization group methods [37, 38, 39] can be applied to this rate equation. From a numerical viewpoint, the exact solution to any reaction scheme can be evaluated for the first few time steps. If this can be carried to a sufficiently high order, then one might hope to extract useful information about the long-time kinetic behavior of the reaction. There have been two noteworthy studies which have followed this general approach [40, 41, 42]. Dickman and Jensen applied the series expansion formalism to the non-equilibrium interacting particle systems, while Song and Poland investigated several generic reaction-diffusion processes. While the latter approach appears to be promising, their series calculation was carried out by hand. Furthermore, the analysis methods used sometimes lacked internal consistency, leading to an uncertain interpretation of the results.

In the following, we describe a systematic approach to obtain time power series for general types of one-dimensional reaction processes. We represent reactions in terms of creation and annihilation operators. We then discuss how to convert the theoretical formalism into a computational algorithm simply by considering the time evolution of small clusters with periodic boundary conditions. Additionally, we develop a simple and relatively direct method to determine the asymptotic behavior of basic physical quantities from the results of the time series expansion. The failure of the ratio method [43] leads us to suggest a direct application of Padé approximants as a method for determining the asymptotic behavior. We exploit the exactly soluble case of single species annihilation to demonstrate the relative utility of the various series analysis methods.

5.3 Theory and Implementation

In this section, we describe how the temporal evolution of a reactive system can be determined in terms of the action of an evolution operator on an initial state. This approach is advantageous since it leads to a linear equation of motion. Thus a formal solution can be written for the state of the system at any given time. The use of the occupation number representation is natural in this formulation and facilitates the numerical evaluation of the coefficients of the exact time power series.

In general, a specific site i can be either empty or occupied by one or more particles. For simplicity, we restrict ourself to models with singly occupied sites, although a generalization to multiple occupancy is possible. In addition, we are interested in situations where there are only a few different species. The state of a single site i will take the symbolic values $|\phi_i\rangle = |o_i\rangle, |a_i\rangle, |b_i\rangle$ *etc.*, to describe an empty site, an A-occupied site or a B-occupied site, respectively. A typical configuration of reactants can be constructed as a product of all the site states $|\Phi\rangle = \prod_i |\phi_i\rangle$. The state of a system may now be written as

$$|\Psi\rangle = \sum_{\Phi} P(\Phi, t)|\Phi\rangle, \tag{5.3}$$

where $P(\Phi, t) = \langle\Phi|\Psi(t)\rangle$ is the probability that the system is in configuration $|\Phi\rangle$ at time t.

The state function $|\Psi\rangle$ obeys a linear equation of motion

$$\frac{\partial}{\partial t}|\Psi\rangle = \mathcal{L}|\Psi\rangle, \tag{5.4}$$

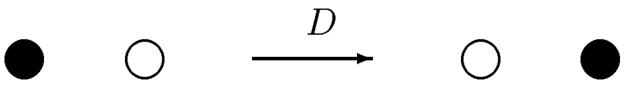

Figure 5.2: The hopping process

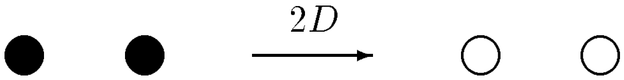

Figure 5.3: The reaction process

where the operator $\mathcal{L} = \sum_{\Phi\Phi'} \mathcal{L}_{\Phi\Phi'}|\Phi\rangle\langle\Phi'|$ enumerates all possible transitions between two configurations. Thus $\mathcal{L}_{\Phi\Phi'}$ is the rate of transition from Φ' to Φ. This evolution operator can be represented in a compact form using creation and annihilation operators. For example, the creation operator for the A species at site i, $A_i^\dagger$, is non-zero only when applied to the empty state, $A_i^\dagger|o_i\rangle = |a_i\rangle$. Similarly, the annihilation operator A_i at site i is non-vanishing when applied to $|a_i\rangle$ only, $A_i|a_i\rangle = |o_i\rangle$.

With these elemental operators, it is now possible to express the effect of the diffusion step and the reaction step on an arbitrary configuration of particles. For example, the situation where all the A particles hop to the right can be represented in terms of the operator

$$\mathcal{L}_{AO} = D\sum_i (1 - A_i^\dagger A_{i+1}) A_i A_{i+1}^\dagger. \tag{5.5}$$

The positive term accounts for hopping from site i to site $i+1$ with rate D, and the negative term corresponding to the loss of probability from site i due to hopping to the right. To be concrete, for the two site configuration $|ao\rangle$, $\mathcal{L}_{AO}|ao\rangle = D(|oa\rangle - |ao\rangle)$, while $\mathcal{L}_{AO}$ yields zero when applied to any other two-site configuration. The operator that corresponds to the actual reaction can also be represented in a similar fashion. For example, for the case of mutual annihilation of two reactive species A and B via the reaction $A + B \to O$, the rate operator for the annihilation process is

$$\mathcal{L}_{AB} = 2D\sum_i (1 - A_i^\dagger B_{i+1}^\dagger) A_i B_{i+1}. \tag{5.6}$$

The factor of 2 accounts for the fact that a hop of either the A or the B in the correct direction leads to an annihilation event. This operator gives a non-zero result only when applied to $|ab\rangle$, that is $\mathcal{L}_{AB}|ab\rangle = 2D(|oo\rangle - |ab\rangle)$. In fact, if only nearest neighbors interact, $\mathcal{L}$ is just a linear combination of operators of the form $\mathcal{L}_{AO}$ and $\mathcal{L}_{AB}$. In other words, a reaction process is well defined by the interaction of a particle with a neighboring empty site and a neighboring particle .

Once the initial state of the system is specified, the state of system at any later time is given by the following formal solution of Eq. (5.4)

$$|\Psi(t)\rangle = e^{\mathcal{L}t}|\Psi(0)\rangle. \tag{5.7}$$

In most cases, an exact solution is hard to obtain, and one is led to expand the state function as a power series around $t = 0$. By defining $|\Psi_j\rangle = \mathcal{L}^j|\Psi(0)\rangle/j!$, the series expansion to the state function takes the form

$$|\Psi(t)\rangle = \sum_{j=0}^{\infty} t^j|\Psi_j\rangle. \tag{5.8}$$

Typical quantities of interest, such as the concentration of a given species or particle correlation functions, can be obtained by evaluating expectation values of a suitably-defined operator. For example, the concentration of the A-species is given by

$$c_A(t) = \frac{1}{N}\sum_{\Phi} N_A(\Phi)\langle\Phi|\Psi(t)\rangle, \tag{5.9}$$

where $N_A(\Phi)$ is the number of A particles in configuration $|\Phi\rangle$.

We now discuss how the aforementioned formalism can be developed into a calculational procedure to provide a numerical evaluation of the time series. The elements of the time evolution operator typically represent interactions between nearest neighbors only, and thus the successive application of the operator j times connects sites which are separated by a distance j. Hence, to obtain a series to the n^{th} order, one can restrict attention to a ring of size $N = n + 1$ with periodic boundary conditions.

It is useful to note that in the case of nearest neighbors interactions only, the rate operator is well defined by its action on all possible pair configurations. Therefore, one may consider the full evolution operator as a superposition of pair operators and then apply the pair operator to all N pairs of a given configuration. Typically, a pair operator is non-vanishing only for a few pairs, and thus a code written for computing series in one process can be converted easily to evaluate the series for another process.

In practice, the number of terms in $|\Psi_j\rangle$ increases exponentially in j, and it is advantageous to classify the initial state and the rate operator in terms of symmetries to optimize the computation. For spatially homogeneous systems, the initial state as well as the rate operator are invariant under discrete rotations, and it is therefore useful to represent rotationally equivalent configurations by only a single configuration. Moreover, processes may obey a conjugation symmetry. For example, in the case of diffusion-limited $A+B \to O$, only states with a majority of A particles need be considered. By taking advantage of these various symmetries, we are able to reach a higher order in the series enumeration.

As an example of the formalism, let us calculate the first three terms in a ballistic annihilation process. In this model one species (A) can hop to the right only, and the other species (B) can hop to the left only. Whenever a particle lands on any occupied site an annihilation event occurs, *i. e.*, mutual reaction as well as self-reaction occur. The rate operator takes the form

$$\mathcal{L} = \mathcal{L}_{AO} + \mathcal{L}_{OB} + \mathcal{L}_{AB} + \frac{\mathcal{L}_{AA}}{2} + \frac{\mathcal{L}_{BB}}{2}, \tag{5.10}$$

with the definitions of Eqs. (5.5) and (5.6). Here $\mathcal{L}_{AA}$ is obtained from $\mathcal{L}_{AB}$ by replacing B with A. Note, however, that self-reaction occurs with half the rate of mutual reaction since a hop of only one of the particles in a same species pair will lead to a reaction. Let us consider an initial state in which each site has the same probability of being occupied by an A or a B. Thus using rotational invariance, the initial state can be written as

$$|\psi_0\rangle = (|aaa\rangle + 3|aab\rangle + 3|abb\rangle + |bbb\rangle)/8. \tag{5.11}$$

By applying the rate operator of Eq. (5.10) twice, one can directly verify that the next two terms in the time series expansion of the state function are,

$$\begin{aligned} |\psi_1\rangle &= 3D(|aoo\rangle + |boo\rangle - 2|\psi_0\rangle)/2 \\ |\psi_2\rangle &= 9D^2(2|\psi_0\rangle - |aoo\rangle - |boo\rangle)/4. \end{aligned} \tag{5.12}$$

Next, by applying Eq. (5.9), we obtain the concentration to second order as,

$$c_A(t) = c_B(t) = 1/2 - Dt + 3(Dt)^2/2 + \cdots \ . \tag{5.13}$$

Although this exercise is quite simple, the number of terms in the $|\Psi_j\rangle$ grows rapidly in j, and the computation is best done systematically by a computer program. The algorithm for calculating the time-series coefficients is described in Appendix D.

5.4 Asymptotic Analysis of the Time Expansion

We are now interested in extracting the asymptotic behavior from the short-time power series representation of observables. In previous studies, this extrapolation procedure was accomplished by direct methods, as well as by using various forms of Padé analysis. Unfortunately, the accuracy and consistency of specific methods varies widely from series to series. Thus many previous approaches incorporate some degree of subjectivity in the analysis. Ideally, this is a feature which one would hope to avoid. We will propose an extrapolation approach which ameliorates subjective aspects to a large extent.

We first consider the analysis of the series for the exactly soluble process $A+A \to O$. We demonstrate how direct application of Padé approximants can serve as a simple yet useful way to determine the asymptotic behavior. The basic question that we shall address is to ascertain the appropriate analysis method for estimating the exponent α in the asymptotic form for the time dependent concentration

$$c(t) \sim t^{-\alpha} \tag{5.14}$$

from the first $n+1$ terms in the series expansion

$$c(t) \approx c_0 + c_1 t + \cdots + c_n t^n. \tag{5.15}$$

To test the utility of any analysis method, we expand the exact solution for the single species annihilation process to an arbitrarily large order and then analyze the series as if the exact solution was not available. For single species annihilation the rate operator takes the form

$$\mathcal{L} = \mathcal{L}_{AO} + \mathcal{L}_{OA} + \mathcal{L}_{AA} \, . \tag{5.16}$$

Using Eqs. (5.5) and (5.6) it is found that the quartic term $A_i^\dagger A_i A_{i+1} A_{i+1}^\dagger$ vanishes, and an exact solution can be obtained via a transformation to Fermion operators [4, 5]. The exact expression for the concentration is

$$c(t) = I_0(4Dt)\exp(-4Dt), \tag{5.17}$$

from which the asymptotic behavior is $c(t) \sim t^{-1/2}$.

We now suggest an alternative and simple method which appears to be better suited for asymptotic analysis than the ratio method. The analysis can be summarized by the following steps:

1. Representing the original function by different Padé approximants.
2. Considering the two approximants which agree over the longest temporal range.
3. Fitting the aforementioned approximants to a power-law function and thereby determining the decay exponent.

For the purpose of asymptotic analysis, it is useful to return to a more basic question and consider the best way to approximate the *concentration*, given the Taylor series of Eq. (5.15). We again consider single-species annihilation and limit ourself to the first 25 series terms, since this is a typical upper limit of what we can attain by the series computation with current resources. A plot of the truncated series for the concentration *vs.* the exact solution given in Eq. (5.17) shows that the Taylor series converges to the exact solution only up to $t \cong 1$ (see Fig. 5.4). If we define a cut-off point τ_0 as the earliest time when the discrepancy between two functions exceeds $\epsilon = 0.001$, we obtain $\tau_0 = 1.1$. Since we are interested in determining the behavior of the concentration in the long-time limit, we see that naïve use of the Taylor series is of limited practical utility in representing the concentration.

-bb-error = =

Figure 5.4: Approximating the time dependence of the concentration from its power series in the case of single species annihilation. (a) Shown are the exact solution (solid), the 25-term Taylor series (dashed) and the $[11,11]$ (dotted) and $[12,12]$ (dashed) Padé approximants.

A significant improvement can be achieved by applying the Padé approximation directly to the time expansion of $c(t)$. That is, we form the rational function

$$P_{[n,m]}(t) = \frac{a_0 + a_1 t + \cdots + a_n t^n}{b_0 + b_1 t + \cdots + b_m t^m}, \tag{5.18}$$

where $b_0 = 1$, and the rest of the $n+m+1$ coefficients are chosen such that the expansions of $P_{[n,m]}(t)$ and of $c(t)$ are identical up to the $n+m^{\text{th}}$ order. Examination of the temporal range where the various Padé approximants converge to the exact solution reveals the utility of this approximation. For the so-called "diagonal approximants" $P_{[n,n]}$, one finds that the approximant and the exact solution agree to within 0.001 up to $\tau_0 = 4.1, 4.5, 4.8, 5.3$ for $n = 9, 10, 11, 12$, respectively (Fig. 5.4). Moreover, at $t = 10$ the $[11,11]$ and $[12,12]$ approximants shown in Fig. 5.4 agree with the exact function up to 10%, while for $t \gtrsim 1.1$ the 25-term Taylor series diverges badly.

Unlike the example above, the original function is usually unknown. However, Fig. 5.4 clearly shows that the exact solution can be well approximated over a substantial temporal range by Padé approximants. A criterion for the time regime over which two different Padé approximants accurately represent a function can be de-

-bb-error = =

Figure 5.5: The fit function $1 - g(\alpha)$ for the $[11, 11]$ (solid) and $[12, 12]$ (dashed) approximants.

veloped by defining a cut-off time $t_0([n, m], [n', m'])$ where the $[n, m]$ and $[n', m']$ approximants first differ by $\epsilon = 0.001$. We consider the two Padé approximants which give the largest value of $t_{\max} = \max\ \{t_0\}$ as the best approximations to the original function. Typically, this analysis extends the convergence of the series well into the asymptotic region and thus enables one to draw conclusions about the long time nature of the decay. Although in the example discussed above, the approximants exhibit a monotonic improvement in convergence as the order is increased, one should be cautious since monotonic convergence does not always occur. Increasing the order of the approximant eventually improves the outcome, but the existence of spurious singularities close to the physical pole in specific Padé approximants may lead to a transitory decrease in the quality of the results.

In our application of the Padé method, we have adopted the following procedure to estimate the exponent governing the long-time decay. We define a quality of fit function $g(\alpha)$ by

$$g(\alpha) = \frac{\langle t^{-\alpha} | P_{[n,m]}(t) \rangle}{\Big(\langle t^{-\alpha} | t^{-\alpha} \rangle \langle P_{[n,m]}(t) | P_{[n,m]}(t) \rangle \Big)^{1/2}}, \tag{5.19}$$

with the inner product $\langle f_1 | f_2 \rangle \equiv \int_{t_1}^{t_2} f_1(t) f_2(t) dt$. This inner product measures how "close" a given Padé approximant $P_{[n,m]}(t)$ is to $t^{-\alpha}$ in the time interval $[t_1, t_2]$, and for a perfect fit one has $g(\alpha) = 1$. The optimal exponent α_{opt} is given by the value that maximizes $g(\alpha)$. There are several constraints concerning the integration interval $[t_1, t_2]$. First, the short-time regime has to be excluded since the concentration does not follow a power law. Second, the cutoff t_2 should be as large as possible in order to minimize the effects of the short-time corrections to the asymptotic decay, but small enough so that the Padé approximant is still accurate. Hence, we use $t_2 = t_{\mathrm{max}}$ with the definition given above and define $t_1 = t_{\mathrm{max}} - 1$ in order to get a uniform integration length. Finally, the two approximants corresponding to the largest value of t_{max} will yield two different exponents, and we average these two values to quote the estimated exponent α_{est}. An averaging procedure is chosen here since it is not possible to determine *a priori* which approximant is closer to the original function.

We now illustrate this fitting procedure by applying it to the known series for the reaction $A + A \to O$. By comparing all possible pairs of approximants given the 25-term time series expansion, we find that $P_{[11,11]}$ and $P_{[12,12]}$ yield the largest value of $t_{\mathrm{max}} = 4.3$. Since the resulting values of $g(\alpha)$ are very close to unity and weakly varying on α, it is useful to locate the minimum of $f \equiv 1 - g$ *vs.* α (see Fig. 5.5). Following this procedure, we find $\alpha_{\mathrm{opt}} = 0.512$ and $\alpha_{\mathrm{opt}} = 0.508$ for the [11,11] and [12,12] approximants, respectively, with the integration range $[3.3, 4.3]$. Thus, we quote the estimated value $\alpha_{\mathrm{est}} = 0.51$ for the decay exponent. This differs by 2% from the exact value $\alpha = 1/2$.

The dependence of the estimated exponents on the fitting procedure can be examined by varying the parameters used. The tolerance parameter ϵ was varied by 10%, and the above analysis showed a 0.01% change in the resulting α_{est}, due to a corresponding change in the integration limits. Moreover, the length of the integration interval was varied by 10%, with the upper limit kept fixed, and in this case the estimated exponent agreed with the original estimate to within 0.02%. These tests demonstrate the weak dependence of the analysis outcome on the fitting parameters.

To demonstrate the rate by which the estimated exponents approach the ultimate value, we performed the aforementioned analysis with a varying order of the time series expansion. The resulting estimated exponents were $\alpha_{\mathrm{est}} = 0.517$, 0.507 and

n	c_n	n	c_n
0	0.500000000000000	9	0.048626063154228
1	−1.000000000000000	10	−0.045346447200260
2	1.500000000000000	11	0.028467120232814
3	−1.666666666666667	12	−0.013827197289845
4	1.416666666666667	13	0.005071234556065
5	−0.935416666666667	14	−0.001031397263083
6	0.468402777777778	15	−0.003347397123149
7	−0.152715773809524	16	0.000536792117891
8	−0.001765581044385		

Table 5.1: Expansion coefficients in the time power series for the concentration for asynchronous ballistic annihilation

0.505 for a Taylor series of the 20, 30 and 40 order, respectively. We conclude that convergence to limiting value does indeed occur, although the rate of convergence is quite slow.

We have applied the series method to several reaction processes, and the utility of the method varied from process to process. For both two and three species diffusive-driven annihilation, reasonable estimates for the decay exponents were found [43]. On the other hand, for some processes the exponent estimates converged slowly towards their long-time limiting behavior. For example, a restricted asynchronous ballistic annihilation model, where self annihilation is excluded, yields poor estimates for the expected decay exponent given the 16th order expansion. Therefore, we conclude that series expansion is not guaranteed to be helpful. Theoretically, if one obtains enough terms the long time behavior will eventually emerge, but this may be beyond the reach of available computing resources.

5.5 Application to Ballistic Annihilation

In this section, we apply the series analysis technique to asynchronous ballistic annihilation model presented in section 5.1. For this reaction process, the rate operator can be written as

$$\mathcal{L} = \mathcal{L}_{AO} + \mathcal{L}_{OB} + \mathcal{L}_{AB} + \frac{\mathcal{L}_{AA}}{2} + \frac{\mathcal{L}_{BB}}{2}, \tag{5.20}$$

where the last two terms account for the self-reaction of particles with the same velocity. We consider an initial state where each particle can assume a velocity $\pm v_0$ with equal probability. The initial state function then equals the sum of all N-particle configurations of velocities divided by 2^N. With our method, we obtain series for the concentration to 16^{th} order (see Table 5.1). The two Padé approximants that agree over the largest temporal range are $[7,7]$ and $[7,8]$, and the upper cutoff time is $t_{\max} = 2.5$ (Fig. 5.6). We do not consider the next diagonal approximant $[8,8]$ since this approximant leads to a reduced temporal range of internal consistency. Thus, we perform the integration over the interval [1.5,2.5]. By maximizing $g(\alpha)$, the values of the optimal exponents are found to be $\alpha_{\text{opt}} = 0.716$ and 0.717 respectively (Fig. 5.7). We conclude an estimated value of $\alpha_{\text{est}} = 0.72$, which yields a 4% deviation when compared with the value $\alpha = 3/4$ suggested by scaling arguments and by Monte-Carlo simulations.

To summarize, we have discussed a ballistic annihilation model where species diffuse in addition to the primary ballistic motion. Using scaling arguments and numerical simulations, we showed that this model belongs to a new universality class. The concentration decays faster than either ballistic annihilation or diffusive annihilation. In the long time limit, the system is governed by two length scales. In the diffusive dominated regime reaction occurs between any two particles while in the ballistic controlled regime, only opposite velocity particles interact. Hence, the system organizes into domains of particles moving with similar velocities. It may prove interesting to analyze the temporal dependence of microscopic properties such as the average distance between two opposite velocities.

To analyze this reaction numerically, we also presented a general method for

-bb-error = =

Figure 5.6: Time dependence of the concentration for the ballistic annihilation model. Shown are the $[7,7]$ (solid), $[7,8]$ (dotted) and $[8,8]$ (dashed) Padé approximants.

-bb-error = =

Figure 5.7: The fit function $1-g(\alpha)$ for the $[7,7]$ (solid) and $[7,8]$ (dashed) approximants.

calculating a power series expansion in time of basic physical quantities, such as the concentration. We have suggested an analysis technique, based on a direct application of the Padé method to obtain the concentration over an extended temporal range. The asymptotic behavior of the series was determined by matching the power series to the two "closest" Padé approximants. Reasonable estimates for the asymptotic behavior of the ballistic reaction were extracted from the time expansion.

Chapter 6

Inhomogeneous Two-Species Annihilation in the Steady State

Bimolecular reactions are encountered in many chemical systems. Typically, two distinct molecules react upon contact and produce a chemically inert product. For example, a recent experiment examined the kinetic properties of the reaction process $I_2 + 2Ag \to 2AgI$ [44]. It is natural to model this system by the two-species reaction process $A + B \to 0$. In section 2.4, this reactive system was considered in the case of homogeneous random initial conditions. The reaction is controlled by spatial fluctuations in the initial conditions, leading to slower than mean-field decay kinetics. A natural way to study the interface between A particles and B particles is to prepare a system with initially separated components and then monitor the reaction rate as a function of time, as first studied by Gálfi and Rácz [45]. This type of geometry is also relatively more amenable to experimental investigation [46, 47] than the more extensively studied homogeneous case [13, 14].

In this chapter we investigate steady-state geometrical properties of the reaction interface when A and B particles are injected at opposite extremities of a finite domain with equal flux j. By balancing the input flux with the number of reactions, we determine that the width w of the reaction zone scales as $j^{-1/3}$ in the large flux limit

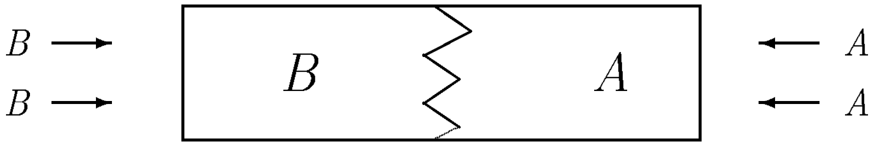

Figure 6.1: Reactants are injected with equal flux at the opposite boundaries of the system.

and that the concentration in this zone is proportional to $j^{2/3}$. This same behavior is deduced from the solution to the mean-field reaction-diffusion equation. In the low flux limit, the concentration is almost independent of position and is proportional to $\sqrt{j}$. In the latter case, the local reaction rate reaches maximum at the edges of the system rather than at the midpoint. When the two species approach at a finite velocity, there exists a critical velocity, above which the reactants essentially pass through each other. Results similar to those in one dimension are found in two- and three-dimensional radial geometries. Finally, we apply the quasistatic approximation to our steady-state solution to recover the known time dependence for the reaction zone width for the case of initially separated components with no external input.

6.1 The Steady State Model

In a mean-field description, the kinetics are described by the reaction-diffusion equations

$$\begin{aligned} \frac{\partial c_A}{\partial t} &= D_A \nabla^2 c_A - k c_A c_B, \\ \frac{\partial c_B}{\partial t} &= D_B \nabla^2 c_B - k c_A c_B, \end{aligned} \tag{6.1}$$

where D_i is the diffusion coefficient of species i, and k is the reaction constant. For the case of initially separated components, the initial conditions are $c_A(x, t = 0) = c_0$ for $x > 0$, and $c_A(x, t = 0) = 0$ for $x < 0$, and conversely for the concentration of B's. On the basis of scaling arguments and through solutions of the reaction-diffusion equation, Gálfi and Rácz [45] found that the width w of the reaction zone increases with time t as $t^{1/6}$, and that the reaction rate vanishes as $t^{-2/3}$.

We discuss here the complementary situation in which particles are confined to a finite d-dimensional bar with equal fluxes of A's and B's injected at opposite ends of the system. Our goal is to understand the geometrical properties of the ensuing steady state. Notice that in the steady state, we can redefine the concentrations by $c_A \Rightarrow D_B c_A$ and $c_B \Rightarrow D_A c_B$ to map the problem to the case of equal diffusion coefficients for the two species. Thus without loss of generality, we posit equal diffusion coefficients for the two species. This system is described by the steady state equations

$$\begin{aligned} D\nabla^2 c_A &= k c_A c_B, \\ D\nabla^2 c_B &= k c_A c_B, \end{aligned} \tag{6.2}$$

with the boundary conditions

$$D c_A'|_{x=L} = j, \quad D c_B'|_{x=L} = 0 \qquad \text{and} \qquad D c_A'|_{x=-L} = 0, \quad D c_B'|_{x=-L} = -j. \tag{6.3}$$

The reflecting boundary condition imposed on the A's at $x = -L$ and on the B's at $x = L$ ensures that the reactants remain within $[-L, L]$. We emphasize that these reaction-diffusion equations provide a mean-field description of the reaction interface in which all spatial fluctuations and the role of the spatial dimensionality are ignored. Within this approximation, we shall determine the extent of the reaction zone and the spatial distribution of the two species.

A rough estimate for these two quantities can be obtained from simple heuristic arguments. Consider first the situation of a large input flux, so that the concentration profile is linear near the domain boundaries with the magnitude of the slope proportional to j/D. If we define the reaction zone as the region for which the concentrations of both species are non-negligible, then the concentration in the reaction zone should be of the order jw/D, where w is the reaction zone width. Consequently, the number of annihilation events per unit time is of order $k c_A c_B w$, which is obtained by integrating the reaction term over the reaction zone. This number should equal the flux of particles j entering the domain. Therefore, balancing these two rates gives

$$kc_A c_B w \sim k\left(\frac{jw}{D}\right)^2 w \sim j, \tag{6.4}$$

or

$$w_0 \sim \left(\frac{D^2}{jk}\right)^{1/3}. \tag{6.5}$$

Thus we conclude that the width of the reaction zone is proportional to $j^{-1/3}$ and that the typical concentration in the reaction zone is

$$c_A, c_B \sim jw/D \sim \left(\frac{j^2}{Dk}\right)^{1/3}. \tag{6.6}$$

These results apply as long as the width w is much less than (and independent of) L. From Eq. (6.5), this corresponds to the flux j being greater than a threshold value j_0, which scales as $j_0 = D^2/kL^3$. When $j < j_0$, the rate balance argument fails, indicative of a different scaling behavior for this case. We will outline an alternative approach for this limiting situation based on the approximate solution to the reaction-diffusion equations (see below).

6.2 Solution to the Reaction-Diffusion Equation

For a quantitative analysis, it is convenient to consider the reaction-diffusion equations for the difference, $c_- = c_A - c_B$, and the sum, $c_+ = c_A + c_B$, from which the behavior of c_A and c_B can easily be inferred. From Eq. (6.3), c_- obeys $c_-(x)'' = 0$, with the boundary conditions $Dc_-(x = \pm L)' = j$. The corresponding solution is $c_-(x) = j(x - x_0)/D$, with x_0 determined by the constraint that the number of A's equals the number of B's in the domain, since the two species are injected and annihilate at the same rate. Thus, imposing $\int_{-L}^{+L} c_-(x)dx = 0$ gives $x_0 = 0$. This condition also specifies the location of the center of the reaction zone. Hence, the concentration difference is

$$c_-(x) = \frac{jx}{D}. \tag{6.7}$$

Using Eq. (6.3), the sum of the concentrations obeys the equation $Dc_+(x)'' = 2kc_Ac_B$, which can be rewritten in a closed form by using $4c_Ac_B = c_+^2 - c_-^2$ to yield,

$$c_+(x)'' = \frac{k}{2D}\left[c_+^2 - \left(\frac{jx}{D}\right)^2\right], \tag{6.8}$$

with the boundary conditions $Dc_+(x = \pm L)' = \pm j$. Since $c_+(x)$ is an even function of x, it is sufficient to consider $x > 0$ only. Notice also that $c_+ \cong c_-$ for positive x outside the reaction zone, since the concentration of the minority species B is negligible in this region. (In fact, the ansatz $c_+ = |c_-|$ satisfies the Eq. (6.8) everywhere, except at the origin.)

For large flux, $j > j_0$, we attempt a power-series solution for $c_+(x)$ in the reaction zone, namely $c_+(x) = c_0 + c_2x^2 + c_4x^4 + \cdots$. Substituting a three-terms series truncation for $c_+(x)$ in Eq. (6.8), we find

$$c_+(x) = \frac{w_0 j}{D}\left[\left(\frac{4}{5}\right)^{1/3} + \left(\frac{1}{10}\right)^{2/3}\left(\frac{x}{w_0}\right)^2 - \left(\frac{1}{40}\right)\left(\frac{x}{w_0}\right)^4\right], \qquad |x| < w, \tag{6.9}$$

with $w_0 = (D^2/jk)^{1/3}$. In general, the coefficient of x^{2n} in the series is proportional to $j/(Dw_0^{2n-1}) \sim j^{2(n+1)/3}$, with the numerical prefactor rapidly converging to a limiting value as more terms in the series approximation of $c_+(x)$ are retained.

We may now determine the reaction zone width by equating c_+ to c_- at $x = w$. Up to the order given in Eq. (6.9), this prescription yields $w \cong 1.179w_0$, in agreement with our previous flux balance argument. From Eq. (6.9), we also find that the concentration in the reaction zone is of the order of $c_0 \propto (j^2/Dk)^{1/3}$. Outside the reaction zone, c_+ matches smoothly with $|c_-|$. It is worth noting that the above results for c_0 and w can be inferred by determining the scaled variables that bring Eq. (6.8) into dimensionless form.

It is instructive to determine the concentration of the minority species outside the reaction zone by direct means. For the concentration of B's at large x, we substitute $c_A = c_B + (jx/D)$ in Eq. (6.3) to give $Dc_B(x)'' = kc_B(c_B + jx/D)$. In the domain $x \gg w$, $c_B(x) \ll jx/D$, and therefore the differential equation reduces to the Airy equation,

$$c_B(z)'' = z\, c_B(z), \qquad z = x/w_0. \tag{6.10}$$

-bb-error = =

Figure 6.2: The high flux limit. Shown are the spatial distribution of the A's and B's (dashed) and the reaction rate R, based on the numerical solution to the steady state reaction-diffusion equation for a system with $j = 100$ and $L = D = k = 1$.

The limiting case $x \gg w$ corresponds to $z \gg 1$, for which the appropriate (decaying) solution is

$$c_B(x) \sim \frac{w_0 j}{D} \left(\frac{w_0}{x}\right)^{1/4} \exp\left(-2(x/w_0)^{3/2}/3\right) . \tag{6.11}$$

In this expression, the prefactor has been chosen to match the small-x power series representation for $c_+(x)$ when $x \cong w_0$.

Thus in the high flux limit, the concentration of B's is approximately $-jx/D$ for $x < -w$ and exponentially small for $x > w$ (Eq. (6.11)). In the reaction zone itself, $|x| < w$, the concentration of B's can be deduced by writing c_B as $(c_+ - c_-)/2$ and using the above expressions for c_+ and c_- in the reaction zone. This yields $c_B \propto j^{2/3}$. The concentration of A's is merely the mirror image of $c_B(x)$ about $x_0 = 0$.

In the low flux limit, $j < j_0$, the approach presented above fails to satisfy the boundary conditions. However, for this case, we exploit the fact that the concentration must be slowly varying in x. Therefore we postulate that $c_+(x) = c_0 + c_2 x^2$ over the entire domain $|x| \leq L$. With this assumption, the boundary conditions on c_+ at $x = \pm L$ now yield $c_2 = j/2DL$. By substituting this form into Eq. (6.8), we then find that the constant c_0 is given by $c_0 = \sqrt{2j/kL}$. With these two leading terms, the remaining terms in an infinite power series representation of the solution

-bb-error = =

Figure 6.3: Particle distribution and reaction rate in the low flux limit. We chose $j = 0.01$ and $D = k = L = 1$.

can be evaluated, and it is straightforward to show that these higher-order terms are negligible. Thus, the approximate form for $c_+(x)$ for $j \ll j_0$ is

$$c_+(x) \cong \sqrt{\frac{2j}{kL}} + \left(\frac{j}{2DL}\right) x^2, \tag{6.12}$$

from which the concentration of each species can be reconstructed by $c_{A,B} = (c_+(x) \pm jx/D)/2$ (Figure 6.2). Notice that the magnitude of the variation in concentration ($\sim j$) is small compared to the value of the concentration itself ($\sim \sqrt{j}$). More precisely, the ratio $(c_+(L) - c_+(0))/c_+(0)$ is proportional to $(j/j_0)^{1/2}$.

A quantity which characterizes the spatial extent of the reaction is the local reaction rate $R(x) \equiv k c_A(x) c_B(x) = k(c_+^2 - c_-^2)/4$. Using the previously-obtained expressions for c_+ and c_-, we find

$$R(x) \propto \begin{cases} (jw)^2 - \text{const.} \times (jx)^2, & j > j_0; \\ \\ j + \text{const.} \times j^{3/2} x^2, & j < j_0; \end{cases} \tag{6.13}$$

with both constants positive, so that the reaction rate exhibits a unimodal to bimodal transition at $j \cong j_0$. For large flux, the reaction rate is sharply peaked around $x = 0$, with a width w_0, but in the small flux limit, particles are more likely to react near the boundary of the domain rather than in the center.

In the limit of vanishing flux, we can, in principle, find the exact expression for the reaction rate. This limit is defined by the average time between the injection of an AB pair, $t_j = 1/j$, being large compared to the average time to diffuse across the domain, $t_D \propto L^2/D$, so that the system is occupied by at most two particles. To solve for the kinetics of the two-particle system, we define $x_1 = L - x_A$ and $x_2 = L + x_B$, where $x_A(x_B)$ is the position of particle $A(B)$. Both variables satisfy $0 \leq x_1, x_2 \leq 2L$, and a reaction occurs whenever $x_1 + x_2 = 2L$. By this formulation, the interacting system is mapped onto a two-dimensional random walk in the first-quadrant triangle $x_1 + x_2 \leq 2L$, with reflecting boundary conditions for $x_1, x_2 = 0$ and absorbing boundary conditions for $x_1 + x_2 = 2L$. To specify the initial conditions, we assume that the input flux at one boundary is uncorrelated with that at the other boundary. Therefore, the first particle attains its asymptotic uniform distribution in the domain before the second particle is injected. For the equivalent two-dimensional problem, this leads to the initial condition $p(x_1, x_2, t = 0) = (\delta(x_1) + \delta(x_2))/4L$. The reaction rate corresponds to the total flux at the absorbing boundary $x_1 + x_2 = 2L$. One way to find this flux is by exact enumeration of the probability distribution for the aforementioned initial distribution of random walks. This method confirms that the reaction rate is indeed bimodal.

6.3 Effect of Relative Drift

An interesting and natural generalization is the situation where the two species have a superimposed drift toward each other with velocity v, as would be the case if the two species where oppositely charged and placed in an external electric field. In the high flux limit, $j > j_0$, the density profile exhibits a boundary layer of order D/v from the reaction center, as long as v is greater than D/L. Outside the boundary layer the concentration of majority species is j/v and that of the minority species is exponentially small. Inside the boundary layer the drift is negligible, and the concentration profile merely reduces to that of the zero drift case in the high flux limit. This approach is valid as long as the boundary layer D/v is larger than the reaction zone width $(D^2/jk)^{1/3}$, or $v < v_0$, with the critical velocity given by

$$v_0 = (Djk)^{1/3}. \tag{6.14}$$

In the high velocity limit, we find the amusing feature that the density profile of each species is highly concentrated near the boundary opposite the entrance point. This result can be understood by first rewriting the reaction-convection-diffusion equation in dimensionless form. Introducing $c_{A,B} = (v^2/Dk)\tilde{c}_{A,B}$ and $x = D\tilde{x}/v$ yields the scaled equations,

$$\begin{aligned} \tilde{c}_A'' + \tilde{c}_A' &= \tilde{c}_A \tilde{c}_B, \\ \tilde{c}_B'' - \tilde{c}_B' &= \tilde{c}_A \tilde{c}_B, \end{aligned} \tag{6.15}$$

with the boundary conditions

$$\begin{aligned} \tilde{c}_A' + \tilde{c}_A|_{\tilde{x}=\tilde{L}} &= \epsilon, \qquad & \tilde{c}_B' - \tilde{c}_B|_{\tilde{x}=\tilde{L}} &= 0, \\ \tilde{c}_A' + \tilde{c}_A|_{\tilde{x}=-\tilde{L}} &= 0, \qquad & \tilde{c}_B' - \tilde{c}_B|_{\tilde{x}=-\tilde{L}} &= -\epsilon. \end{aligned} \tag{6.16}$$

The scaled flux $\epsilon = \tilde{j} = (v_0/v)^3$ is vanishingly small when $v > v_0$. To leading order, then, the input is zero, and this implies that the reaction term must vanish, as can be seen by integrating Eq. (6.15) over the length of the box and using the boundary conditions. This fact suggests a perturbative approach, namely $\tilde{c}_A = \tilde{c}_{A0} + \epsilon \tilde{c}_{A1} + \cdots$ and $\tilde{c}_B = \tilde{c}_{B0} + \epsilon \tilde{c}_{B1} + \cdots$. Solving for $\tilde{c}_A$ gives $\tilde{c}_A = c_0 \exp(-\tilde{x} - \tilde{L})$ in the vicinity of $-\tilde{L}$ and $\tilde{c}_A$ vanishing elsewhere, and conversely for the B's. Thus the particles are confined to a boundary layer whose width is of order unity in scaled units where $\tilde{L} = Lv/D \gg 1$. This zero-order solution can be used in Eq. (6.15) to obtain the corrections to this leading behavior. Transforming back to the initial variables, we find, to leading order, that the density is proportional to v^2/Dk within a boundary layer of order D/v, and that corrections are of the order j/v. This gives a reaction rate which is strongly peaked near the boundaries of the box. In the low flux limit, we find that this same behavior still applies as long as $v > D/L$.

6.4 Radial Geometries in Higher Dimensions

We can also determine the nature of the reaction zone in a higher-dimensional analog of the finite linear domain. Consider the radially symmetric situation in which the reaction takes place between two concentric hyperspherical shells of different radii, with A's injected at the outer radius and B's injected at the inner radius. The concentration depends on r only, and the corresponding boundary conditions are $Dr_A^{d-1}c_A(r_A)' = j$, $Dr_B^{d-1}c_A(r_B)' = 0$, and $Dr_B^{d-1}c_B(r_B)' = -j$, $Dr_A^{d-1}c_B(r_A)' = 0$. The equation for the concentration difference is

$$\frac{1}{r^{d-1}}\frac{\partial}{\partial r}\left(r^{d-1}\,\frac{\partial c_-(r)}{\partial r}\right) = 0, \tag{6.17}$$

which, together with the boundary conditions, gives

$$c_-(r) = \begin{cases} \frac{j}{D}\,\log(r/r_0) \quad \text{with } r_0 = \exp\left(\frac{a^2\log a - b^2\log b}{a^2-b^2} - \frac{1}{2}\right) \quad d=2 \\ \\ \frac{j}{D}\left(\frac{1}{r_0} - \frac{1}{r}\right) \quad \text{with } r_0 = \frac{2(a^3-b^3)}{3(a^2-b^2)} \quad d=3 \end{cases} \tag{6.18}$$

As in the one dimensional case, the position of the reaction zone center is determined by requiring that $\int_{r_B}^{r_A} c_-(r)\,r^{d-1}dr = 0$. When both radii are large with their difference remaining finite, then $r_0 \cong (a+b)/2$. However, if the inner radius is much smaller than the outer radius, then $r_0 \cong a/\sqrt{e}$ for $d=2$ and $r_0 \cong 2a/3$ for $d=3$. The procedure for finding the individual concentrations of each species closely follows that used for the one dimensional case. In the high flux limit, c_+ is simply equal to $|c_-|$ outside the reaction zone, and c_+ has a power series representation (which is not necessarily even about r_0) within the reaction zone. Following the same method of analysis as in one dimension, we find the same scaling behavior, namely, $w \sim j^{-1/3}$ and $c(r=r_0) \sim j^{2/3}$. Similarly, in the low-flux limit, we find that the concentration scales as $c \sim \sqrt{j}$, and that the magnitude of the spatial variation of c is of order j.

6.5 The Time-Dependent Problem

By applying the quasi-static approximation to our description of the steady-state, we can also determine the time dependence of the width of the reaction zone in the Gálfi-Rácz problem, where the two components are initially separated and with no external source of particles. The basis of this approximation is to neglect the time derivative in the diffusion equation and shift this time dependence to a moving boundary condition [48]. For the Gálfi and Rácz problem, the growing depletion layer is the source of the moving boundary which produces the requisite time-dependent flux. For the initial conditions $c_A(x,t=0) = c_0 H(x)$ and $c_B(x,t=0) = c_0 H(-x)$, with $H(x)$ the Heaviside step function, and taking $D_A = D_B = D$ in Eq. (1), then $c_-(x,t)$ satisfies $\dot{c}_- = Dc''_-$, with the corresponding initial condition $c_-(x,t=0) = c_0(2H(x)-1)$. The solution of this equation is

$$c_-(x) = c_0 \,\mathrm{erf}\Big(\frac{x}{2\sqrt{Dt}}\Big), \tag{6.19}$$

with the error function defined by $\mathrm{erf}(y) = \frac{2}{\sqrt{\pi}}\int_0^y \exp(-u^2)du$. This solution leads to a depletion zone of the order of $\sqrt{Dt}$. The (time-dependent) flux into the reaction zone is thus given by $j(t) \sim Dc_-(x=0,t)' \sim Dc_0/\sqrt{Dt}$. We now use this flux in the steady-state expression for w (Eq. (6.5)). This yields $w \sim (D^3t/k^2c_0^2)^{1/6}$, in agreement with the Gálfi and Rácz result. *A posteriori*, using the high-flux limit is appropriate, since the flux $j \sim t^{-1/2}$ is much greater than $j_0 \sim L^{-3} \sim t^{-3/2}$.

This $t^{1/6}$ growth of the reaction zone width was confirmed numerically in two-dimensions [49]. However, the corresponding exponent in one dimension remains controversial. Numerical simulations [50] suggest the value 0.30, while a dimension analysis supports the value 1/4 [51]. In one dimension, the reaction constant diverges as the flux vanishes, and therefore the width is independent of k. As a result, one has $w \sim (D/j)^{1/2}$, and the above quasistatic approximation yields $w \sim (Dt/c_0^2)^{1/4}$. Interestingly, the nearest-particle distance of diffusing particles from a trap exhibits the same kinetic behavior in one dimension. For a diffusing reactant, a potential reaction partner is effectively a trap, and it is natural to assume that the interface width and the AB distance follow the same kinetic behavior. The aforementioned dimension analysis also shows that the critical dimension of the system is two, $d_c = 2$ [51]. Hence, the analysis to the reaction-diffusion equation we presented holds for spatial dimension larger or equal to two.

Chapter 7

Collective Properties of Adsorption-Desorption Processes

The adsorption of large particles such as colloids, proteins, latex spheres, *etc.* on solid substrates is typically an irreversible process [52, 53]. A specific example for such a process is the oxidation of Fe(100) by water adsorption [54, 55]. Indeed, in a number of situations, the energetic barriers for desorption are much higher than the corresponding barriers for adsorption. Moreover, particles cannot adsorb on top of previously adsorbed ones. In the review section, we discussed several features of nonoverlapping random sequential adsorption (RSA). In arbitrary dimension, RSA processes reach a jamming configuration, where further adsorption events are not possible. The final coverage as well as the temporal approach to the jammed state are of interest [53, 56, 57, 58, 59, 60, 61]. In Appendix B we derive analytical results for the one dimensional case, where the problem is also known as the "parking" problem [60, 61].

It is clear that the usual RSA model provides an oversimplified description of actual adsorption processes. A more realistic treatment should incorporate various effects such as the transport properties of the particles, the interaction between particles, and possible desorption from the substrate to the bulk [8, 62, 63, 64, 65, 66]. Very recently, RSA models where particles diffuse in the bulk and adsorb on the substrate were considered. Interestingly, introduction of bulk transport did not change the coverage and the structure of the jammed configuration. However, it was found that the approach to the jamming limit depends on the transport properties of the particles [62, 63].

In this chapter, we study the influence of desorption on the one-dimensional parking problem. Such a generalization is appropriate for describing protein binding on a surface [67, 68, 69, 70, 71, 72]. Allowing desorption makes the process manifestly reversible, and the system ultimately reaches an equilibrium state. We solve for the equilibrium properties and find a weak logarithmic dependence of the final coverage on the adsorption rate, in the desorption-controlled limit. To study the kinetics in this limit, we focus on an irreversible model with an infinite rate of adsorption and a finite rate of desorption. A heuristic argument as well as numerical simulations show that the coverage slowly approaches saturation, $1-\rho(t)\sim 1/\log(t)$.

7.1 The Reversible Parking Problem

In the irreversible parking problem, identical particles park on a line with an adsorption rate k_+. Particles attempt to park with an equal rate everywhere, and a parking attempt fails if the space is partially occupied by a previously adsorbed particle. The parking attempt illustrated in Figure 7.1 is thus rejected. We are interested in the more general situation where particles are also allowed to desorb with a desorption rate k_-. Particles desorb regardless of their local environment. The system ultimately reaches an equilibrium state independent of the initial conditions. The primary aim of our study is to describe this final state and the asymptotic approach towards it. To this end we will apply the empty interval distribution method [67]. This technique is often applied to RSA problems, since simple and closed equations emerge. We generalize these equations to describe the reversible case and solve the static equations.

Denote the density of empty intervals of size exactly equal to x at time t by

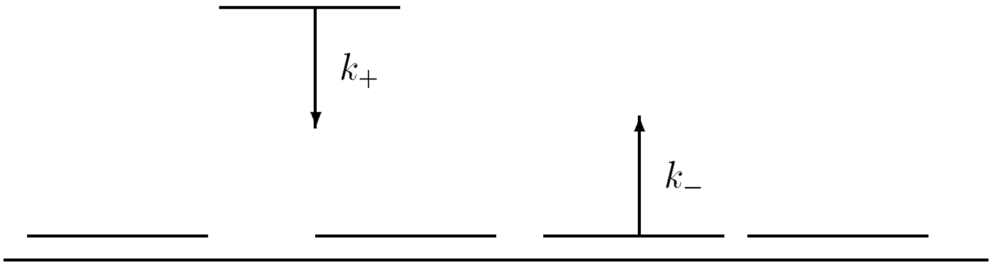

Figure 7.1: Illustration of the adsorption-desorption process.

$P(x,t)$. Each empty interval borders a particle to its left and to its right. Since in the adsorption-desorption process, one interval corresponds to one particle, and since the total density of particles and intervals is equal to unity, one has

$$1 = \int_0^\infty dx\,(x+1)P(x,t). \tag{7.1}$$

Without loss of generality the size of particles is taken as the unit of length. Moreover, from the same one-to-one mapping between particles and intervals, the density of particles can be obtained from the distribution function of empty intervals as

$$\rho(t) = \int_0^\infty dx P(x,t). \tag{7.2}$$

To write the evolution equations one has to account for all possible processes leading to a change of $P(x,t)$. For $x < 1$, an interval disappears when either one of its neighboring particles desorbs. On the other hand, an interval of size x is created when a particle parks at one of two specific locations on an interval of size y with $y > x+1$. These two processes give rise to the following integro-differential equation for $P(x,t)$

$$\frac{\partial P(x,t)}{\partial t} = -2k_- P(x,t) + 2k_+ \int_{x+1}^\infty dy P(y,t), \qquad x < 1. \tag{7.3}$$

Due to adsorption, intervals with length larger than a particle size are destroyed with a rate $k_+(x-1)$. In addition, two neighboring intervals can create a larger interval when the intervening particle desorbs. However, the mere knowledge of the interval distribution function is not sufficient for writing the rate equations. We introduce the interval-interval distribution function $P(y,z,t)$, defined as the density of pairs of neighboring intervals of length y and z which are separated by a single particle. We further assume that this interval-interval distribution function is proportional to the product of single interval densities. This assumption, also known as the independence principle, has proved to be exact in a number of RSA problems [68, 69]. With this assumption, one finds for the rate equation for $x > 1$

$$\begin{aligned}\frac{\partial P(x,t)}{\partial t} &= -2k_- P(x,t) + 2k_+ \int\limits_{x+1}^{\infty} dy P(y,t) \\ &+ \frac{k_-}{\rho(t)} \int\limits_{0}^{x-1} dy P(y,t) P(x-1-y,t) - k_+(x-1)P(x,t).\end{aligned} \qquad x > 1 \qquad (7.3)$$

The convolution term in Eq. (7.3) involves the probability of finding a y interval, $P(y,t)$ and the normalized probability for its neighbor to be of size $x-1-y$, *i. e.*, $P(x-1-y)/\int_0^\infty dx P(x,t)$.

To verify that these equations satisfy the normalization condition of Eq. (7.1) , one can check integrating of Eq. (7.3) that the time derivative of $\int_0^\infty dx\,(x+1)P(x,t) = 0$ vanishes. Another useful check of self-consistency of the rate equations is provided by the integration of the rate equations over all lengths. This gives the equation describing the change of the density,

$$\frac{d\rho(t)}{dt} = -k_- \rho(t) + k_+ \int\limits_{1}^{\infty} dx\,(x-1)P(x,t), \qquad (7.4)$$

which can also be derived directly from the definition of the gap distribution. Equation (7.4) is a generalization of the Langmuir mean-field equation, $d\rho/dt = -k_-\rho + k_+(1-\rho)$, which is recovered by setting the integral on the right-hand side equal to $1-\rho(t)$.

The steady-state interval distribution has to satisfy the static version of Eq. (7.3), that is, both sides of the equation vanish. Interestingly, the simplest attempt, trying the Poissonian distribution $P_{eq}(x) = \beta \exp(-\alpha x)$, is successful. We emphasize that despite the two different equations for $x < 1$ and $x > 1$, the solution is smooth at

-bb-error = =

Figure 7.2: The density of particles in the steady-state of the reversible adsorption-desorption problem. $\rho_{eq}(k_+/k_-)$ is plotted vs. k_-/k_+ for $k_+ > k_-$ (solid line) and vs. k_+/k_- for $k_- > k_+$ (dotted line).

$x = 1$. From the normalization condition of Eq. (7.1) the prefactor is determined to be $\beta = \alpha^2/(1+\alpha)$, while from Eq. (7.2) the value of α is found via a transcendental equation involving k_+/k_-. One can now write the exact steady-state solution as

$$P_{eq}(x) = \frac{\alpha^2}{1+\alpha} \exp\left(-\alpha x\right) \qquad \text{with} \qquad \alpha \exp(\alpha) = k_+/k_-. \tag{7.5}$$

To obtain the density of particles in the steady-state, we use the correspondence between particles and intervals expressed in Eq. (7.2). Hence, it is easily found that $\rho_{eq} = \alpha/(1+\alpha)$. In the desorption-controlled regime, $k_+/k_- \gg 1$, one finds $\alpha \simeq \log(k_+/k_-)$, and consequently,

$$\rho_{eq} \cong 1 - \frac{1}{\log(k_+/k_-)} \qquad k_+/k_- \gg 1. \tag{7.6}$$

Notice that in the limiting case $k_+/k_- \to \infty$, the line is completely filled with particles at the steady state, in contrast to the case of no desorption where asymptotic coverage is $\rho_{\text{jam}} \cong 0.7475$, as derived in Appendix B. However, as the adsorption rate increases while the desorption rate is kept fixed, the coverage increases very weakly, since the corresponding correction is logarithmic. Moreover, the gap distribution is regular at the origin, contrary to the logarithmic divergence occurring in the irreversible case. Thus, the presence of desorption, even if slight, significantly changes the long-time behavior. Note also that in the adsorption-limited case, the coverage displays an obvious linear dependence on the rate ratio, $\rho_{eq} \cong \alpha \cong k_+/k_-$.

To test the theoretical predictions, we performed Monte-Carlo simulations of the reversible parking process. We found that the equilibrium properties are essentially identical to the analytical results shown in Figure (7.2). We also confirmed the Poissonian nature of the density of empty intervals. Furthermore, the relaxation to the steady state has been investigated. As expected, the approach to the steady state coverage is exponential $\rho_{eq} - \rho(t) \propto \exp(-t/\tau)$, where the relaxation time τ appears to be proportional to k_+/k_- with possible logarithmic corrections. For reference, we show in Appendix B that the corresponding approach to the jammed state in the irreversible case has a power-law dependence on time $\rho_{\rm jam} - \rho(t) \propto t^{-1}$. The distribution function $P(x,t)$ exhibits a transient discontinuous derivative at $x = 1$ due to the discontinuous structure of Eq. (7.3) . That feature does not permit us to construct an analytic solution for the time dependent problem.

We now outline the solution for the lattice version [70, 71] of the reversible parking problem. In this model, objects occupy r lattice sites and will be referred to as r-mers. Analogous to the continuous case, r-mers land uniformly on a lattice with a rate k_+ and adsorb if all sites are empty. We define $P(m,t)$ as the density of empty intervals of exact length m. The equivalent to Eqs. (7.1)-(7.3) simply follows, and we merely quote the final results. The density of empty intervals is again Poissonian

$$P_{eq}(m) = \frac{(1-\lambda)^2}{\lambda + r(1-\lambda)}\,\lambda^m \qquad \text{with} \qquad \frac{\lambda^r}{1-\lambda} = \frac{k_-}{k_+}. \tag{7.7}$$

Using the equivalent of Eq. (7.2) $\rho_{eq} = r\sum_0^\infty P_{eq}(m)$, we can find the steady state coverage

$$\rho_{eq} = \frac{r(1-\lambda)}{\lambda + r(1-\lambda)}. \tag{7.8}$$

In the desorption-controlled case, $k_+/k_- \gg 1$, we find that $\rho_{eq} = 1 - (k_-/k_+)^{1/r}/r$. As the size of the r-mer increases, the exponent of the power-law r^{-1} decreases, and ultimately the aforementioned logarithmic nature is reached. Indeed, the solution to the continuous case given by Eqs. (7.5) and (7.6) can be found from Eq. (7.7) by taking the proper limits $x \to m/r$ and $k_+ \to k_+/r$.

7.2 Dynamics in the Desorption-Controlled Limit

The second part of our study focuses on the dynamical properties of the system in the desorption-controlled limit. To attain this regime, immediate adsorption ($k_+ = \infty$) is imposed while the desorption rate is kept finite. Redefining the time $t \to k_- t$, corresponds to taking the desorption rate equal to unity. The evolution may be divided into two stages. First, the system instantaneously reaches a jammed state and then desorption comes into play. Since neither the final coverage nor the asymptotic behavior do not depend on the initial conditions produced at the end of first stage, one can use any initially jammed configuration satisfying the normalization constraint of Eq. (7.1). In the simulations, we have chosen a distribution where all gaps between particles are equal to x_0 with $x_0 < 1$,

$$P(x, t = 0) = \frac{\delta(x - x_0)}{1 + x_0}. \tag{7.9}$$

Once a desorption event has occurred, either one or two adsorption events are possible depending on the length of the two intervals bordering the particle. We have adopted a natural scheme where the first particle lands on a randomly picked segment in the open interval, and then, if feasible, the second particle lands randomly on the remaining interval. Thus, after each desorption and subsequent adsorption event(s) the number of particles is either left unchanged or increases by one. Numerical simulations indicate that this process approaches complete coverage in the long-time limit.

A simple heuristic argument explains the behavior of the system near saturation. Let us imagine that a segment of length $L = N + 2$ is occupied by N particles. Consider a typical situation where the gaps between the particles are comparable ($\sim 1/N$). A successful density-increasing adsorption event may take place only as a result of a number of ordered cooperative desorption-adsorption events. First, the leftmost particle has to desorb and then adsorb near the left end of the segment. Second, the next leftmost particle has to desorb and then adsorb near the right side of the previous particle, *etc.* Finally, a gap larger than the unit length is cleared at the right edge of the segment, and an additional particle successfully adsorbs. The probability for the first event is R/N, since the leftmost particle is desorbed first among N particles. The probability for the second event is $R/(N-1)$ and so forth. The factor $R < 1$ accounts for the probability that the corresponding adsorption event happens in the proper location. The total probability for the cooperative event can be written as $p \sim R^N/N!$. We can now evaluate the time dependence of $N(t)$. The time required for a unit change in N is inversely proportional to p, and one has

$$\frac{dN}{dt} \propto \frac{\Delta N}{\Delta t} \propto p \propto \left(\frac{eR}{N}\right)^N . \tag{7.10}$$

In the last step the Stirling's formula $N! \sim (N/e)^N$ was used. Solving Eq. (7.10) yields the following asymptotic relation for $N(t)$, $N \sim \log(t)/\log(\log(t))$. Since the uncovered fraction obeys $1-\rho(t) \propto 1/N$, an unexpectedly slow long-time behavior of the density emerges,

$$1-\rho(t) \propto \frac{\log(\log(t))}{\log(t)}. \tag{7.11}$$

We describe now a complementary argument that also predicts inverse logarithmic behavior but without the double logarithmic correction. We observe that when the system approaches to the completely covered state, the time interval between successive density-increasing adsorption events increases. Hence, the system has time to "equilibrate" and one can approximate the gap distribution by the Poissonian equilibrium distribution $P(x,t) = \alpha^2 \exp(-\alpha x)/(1+a)$. To solve for the density we write Eq. (7.4) with a vanishing desorption term

$$\frac{d\rho(t)}{dt} = \int_1^\infty dx\,(x-1)P(x,t) = \frac{1}{1+\alpha}\exp\left(-\alpha\right). \tag{7.12}$$

On the other hand, one has $\rho(t) = \alpha/(1+\alpha)$ from Eq. (7.2), and consequently, the time derivative of the density can be expressed as $d\rho(t)/dt = (d\alpha/dt)/(1+\alpha)^2$. By equating the two expressions obtained for $d\rho(t)/dt$ we have

$$\frac{d\alpha}{dt} = (1+\alpha)\exp(-\alpha). \tag{7.13}$$

Solving this differential equation, we arrive at the asymptotic behavior of the density, that is, $\alpha \propto \log(t)$ and

$$1-\rho(t) \propto \frac{1}{\log(t)}. \tag{7.14}$$

-bb-error = =

Figure 7.3: Monte-Carlo simulation results for the infinite adsorption case. The simulation was performed on a ring of length 100,000. (The temporal approach to the fully occupied state. Shown are $f(t)$, $f(t) = (1 - \rho(t)) \log(t)$ vs. t (circles) and $f(t)/\log(\log(t))$ vs. (t) (squares).

Both estimates predict that the desorption-limited process gives rise to a very slow inverse logarithmic approach to the completely covered state. Thus we conclude that in the desorption-controlled limit the dynamics of the system exhibits "glassy" relaxation.

Numerical simulations of the desorption-limited process were performed using the following simple procedure. A list of intervals $\{l_i < 1\}$ is kept, while the locations of the particles are ignored. A simulation step consists of choosing randomly a pair of neighboring intervals, $\{l_i, l_{i+1}\}$. Then the total length $l_i + l_{i+1}$ is redivided randomly to two new intervals, $\tilde{l}_i$ and $\tilde{l}_{i+1}$. If one of these new intervals is larger than unity, an additional particle adsorbs. If $\tilde{l}_i > 1$, for example, two new intervals are created randomly with their total length equal to $\tilde{l}_i - 1$. Time is updated after each event by the inverse of the total number of intervals in the system. To verify the predicted logarithmic approach to the saturated state, we write $f(t) = (1 - \rho(t)) \log(t)$. The simulation results for $f(t)$ and $f(t)/\log(\log(t))$ are shown in Figure 7.3. Both functions are slowly varying in time. Since the former is an increasing function and the latter a decreasing one, we conclude that the estimates (7.11) and

-bb-error = =

Figure 7.4: Monte-Carlo results for the gap distribution at the 65536 time step.

(7.14) provide the upper and lower bounds for the uncovered fraction, respectively. It seems that the upper bound provides a slightly better approximation for $f(t)$.

In Figure 7.4, we present Monte-Carlo simulational results for the gap distribution function. In the long-time limit, the gap distribution function appears to be again Poissonian, at least over a significant range of the gap size. We believe that this supports the argument leading to the lower bound of Eq. (7.14). However, the tail of the distribution, crucial for the adsorption of new particles, cannot be determined from these data.

The success of the Poissonian approximation suggests that the process is mean-field in nature. To check this feature, a mean-field variant of the above Monte-Carlo simulation was also considered. In this model, the two randomly chosen intervals are not required to be neighbors. In fact, the pair is chosen randomly from all available pairs. Simulations have shown little quantitative change and practically no qualitative change in the data similar to those presented on Figure 7.3. We performed other numerical experiments including, *e. g.*, computation of the pair correlation function. Again, simulational results revealed an excellent agreement between the one-dimensional and the mean-field versions.

7.3 Discussion

We have considered near saturation properties of two one-dimensional adsorption-desorption processes. In the reversible case, we have obtained an exact solution that exhibits a slowly varying dependence of the coverage versus the rate ratio k_+/k_-, when $k_+ \gg k_-$. In the case of immediate adsorption, the system slowly approaches the completely covered state. In a configuration where the coverage is large, $\rho \lesssim 1$, a growing number of cooperative desorption-adsorption events are necessary for an additional adsorption to occur. Moreover, the slow nature of the process allows for perfect mixing of different gaps and hence leads to a Poissonian distribution of gaps.

The situation found in this adsorption-desorption process is reminiscent of that encountered in the Ising Model where the phase transitions occur at zero temperature (see chapter 2). Indeed, noting that in the parking problem the rate ratio k_+/k_- plays the role of temperature, we conclude that all basic features of the reversible model such as disordered steady state and exponential approach towards equilibrium correspond to typical behaviors above the point of phase transition. In the desorption-controlled case, the system reaches the perfectly ordered final state while the approach towards it shows a critical slowing down. Furthermore, this analogy suggests that in the two-dimensional case a phase transition in the adsorption-desorption system may take place at a finite k_+/k_-. The desorption-controlled limit in two dimensions seems very interesting since the system can reach numerous metastable states which include, *e. g.*, two ordered perfect crystal structures, triangular and square, and a number of polycrystalline structures with a network of defects. Metastable states should be responsible for slow "glassy" relaxation and sensitivity to initial conditions.

Chapter 8

Cluster Approximation for the Contact Process

The contact process (CP) is an irreversible lattice model involving nearest neighbor interactions only [73, 74]. The model incorporates spontaneous desorption and nearest-neighbor induced adsorption. This stochastic process can be used to mimic epidemic spread as well as catalytic reactions. The model belongs to a general class of nonequilibrium models exhibiting a continuous phase transition. Near the critical point, the system exhibits divergence of spatial and temporal correlations. Such properties, conveniently characterized by critical exponents, can be used to classify different models. The CP belongs to the same universality class as Sclögel's first model [75], Reggeon field theory [76], directed percolation [77], and the ZGB model [78] of catalysis. Field theoretic renormalization group studies [79, 80] provide considerable understanding of the critical behavior of the CP. However, the best estimates for the characteristic exponents were found numerically by Monte Carlo simulations [81] and by series expansion analysis [40, 41].

Motivated by the incomplete theoretical understanding, we introduce an approximate approach to the CP. We study the temporal evolution of the density of empty intervals. The corresponding rate equations lead to an infinite hierarchy of equations.

By writing the density of pairs of neighboring empty intervals as a product over single interval densities, we obtain a closed set of equations. We use the generating function technique to obtain the steady-state properties of the system. Within this approximation, the system exhibits a discontinuous phase transition from an active state to an empty state. As the system approaches the critical point, the relaxation time, associated with the temporal approach to the final state, diverges. Consequently, at the critical point, an anomalously slow decay towards the final state takes place. We find the corresponding kinetic exponent by scaling techniques, as well as by numeric integration of the rate equations.

We compare the cluster approximation predictions with the results of site mean-field theory and with series analysis of this process. Despite the failure to predict a continuous transition, the cluster approximation provides a good approximation for the final density and the empty interval density for a reasonable range of desorption rates. Moreover, the resulting estimates for the critical exponents are closer to the numeric values in comparison with site mean-field theory. The cluster approach is also applicable to generalizations of the contact process, such as the A model and the N3 model. We verify that the resulting critical behavior of these processes is identical with the contact process. Our approach is advantageous since it can be improved systematically by considering the evolution of higher order empty interval densities.

8.1 Steady-State Properties

In the CP, a particle desorbs spontaneously with rate λ. On the other hand, a particle adsorbs at a given site at a rate proportional to the number of neighboring occupied sites. In other words, the adsorption rate at a particular site is given by n_p/n_s, with n_s the total number of neighboring sites and n_p the number of neighboring particles. Since every neighboring particle contributes independently to the adsorption rate, this stochastic process can viewed as an interacting particle system with nearest-neighbor interactions only. The above process possesses an adsorbing

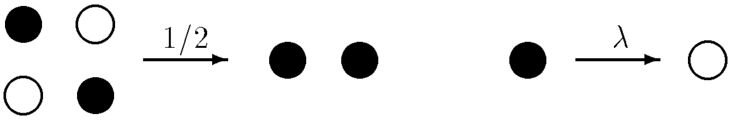

Figure 8.1: The Contact Process.

"vacuum" state: once the system reaches the empty state, adsorption becomes impossible. In sufficiently high dimensions, neighboring sites are not correlated, and the density follows from $d\rho/dt = \rho(1-\rho) - \lambda\rho$. The adsorption term represents the density of vacant sites that neighbor an occupied site. This site mean-field theory (SMF) gives a steady state concentration equal to $1-\lambda$. Hence, at $\lambda_c = 1$ this process undergoes a simple continuous transition.

We consider the one-dimensional case only (see Figure 8.1), where studying the density of empty interval has proven useful in adsorption processes [67], as well as in reaction processes [6]. Denote by $E_n(t)$ the probability that a randomly chosen string of n sites is empty (see Figure 8.2). We emphasize the fact that the actual empty string might be of length larger than n. Let us also consider $R_n(t)$, the probability that a random string of length $n+1$ has n consecutive vacant sites and a particle at the extreme right site. For symmetric processes, such as the CP, $R_n(t)$ also represents the probability of finding an empty string with a particle at the extreme left. These two interval densities are related by

$$R_n = E_n - E_{n+1} \qquad \text{or} \qquad E_n = 1 - R_0 \cdots - R_{n-1}, \tag{8.1}$$

for $n \geq 0$. For $n = 0$, the definition of E_n is trivial, leading to the following conditions satisfied by the empty interval densities,

$$E_0 = 1 \qquad \text{or} \qquad \sum_{n=0}^{\infty} R_n = 1. \tag{8.2}$$

The condition for R_n is obtained by using Eq. (8.1) and noting that the sum over E_n reduces to an alternating series. The above interval densities are useful in describing macroscopic properties; for example, the concentration is given by $\rho(t) = R_0(t)$.

We write the rate equations governing $E_n(t)$ by considering the adsorption and the desorption processes separately. Adsorption can contribute only to loss of empty

$$E_n = \text{Prob}(\underbrace{\circ \;\cdots\; \circ}_{n}) \qquad R_n = \text{Prob}(\underbrace{\circ \;\cdots\; \circ}_{n}\bullet)$$

Figure 8.2: Empty interval densities

intervals. Empty intervals of length n can be destroyed when a particle is desorbed at the edge of the interval. This occurs only where the empty interval has an occupied site at its edge. By taking into account contributions from adsorption at either boundary, we find $dE_n/dt|_{\text{ads}} = -R_n$. Desorption, on the other hand, leads only to the creation of empty intervals. When a particle desorbs, the two empty intervals it borders create a larger empty interval. We define the pair density $E_{l,m}$ as the density of two neighboring empty intervals, with lengths at least equal to l and m, separated by a single particle. Note that from this definition the relation $E_{0,n} = E_{n,0} = R_n$ is satisfied. In terms of this pair density, the increase in the density of empty intervals of length at least n due to desorption is described by $dE_n/dt|_{\text{des}} = \lambda \sum_{l=0}^{n-1} E_{l,n-1-l}$. We then approximate the pair density, $E_{l,m}$, by the product $E_{l,m} \cong R_l R_m / R_0$, where the factor $1/R_0$ ensures the normalization condition $E_{0,n} = R_n$. Combining contributions from both adsorption and desorption yields the following rate equation for the empty interval density,

$$\frac{dE_n}{dt} = -R_n + \frac{\lambda}{R_0} \sum_{l=0}^{n-1} R_l R_{n-1-l}, \qquad n > 0. \tag{8.3}$$

The steady-state properties can be obtained by requiring that the time derivative in Eq. (8.3) vanishes. We introduce the generating function $R(z) = \sum_n R_n z^n / R_0$, with R_n being the steady-state interval densities. Dividing Eq. (8.3) by R_0, summing over all n, and solving the resulting quadratic equation yields

$$R(z) = \frac{1 - \sqrt{1 - 4\lambda z}}{2\lambda z}, \qquad \lambda < 1/4. \tag{8.4}$$

The normalization condition of Eq. (8.2) shows that $\rho = R_0 = 1/R(z)|_{z=1}$ and, consequently, the concentration is given by

$$\rho = \frac{1 + \sqrt{1 - 4\lambda}}{2}, \qquad \lambda < 1/4. \tag{8.5}$$

For $\lambda > \lambda_c = 1/4$ the system indeed exhibits a transition to the absorbing state, where the concentration vanishes. The nature of this transition is discontinuous,

-bb-error = =

Figure 8.3: The cluster approximation density (solid) *vs.* the actual CP density (dashed). The latter density represent the [12,12] Padé approximant obtained from the perturbation study of ref [41].

while for the actual CP, the transition is continuous. For the CP, the approach to the critical density is an algebraic one,

$$\rho - \rho_c \sim (\lambda_c - \lambda)^\beta. \tag{8.6}$$

Note that while for a continuous transition to a vacuum state one has $\rho_c = 0$, the critical density of the cluster approximation is finite, $\rho_c = 1/2$. Extensive power series studies suggest $\beta \cong 0.277$, and $\lambda_c \cong 0.3032$ [40, 41]. The corresponding values obtained by the cluster approximation, $\beta = 1/2$ and $\lambda_c = 1/4$, are closer than the SMF values $\beta = \lambda_c = 1$. While the critical point depends heavily on the microscopic definition of the process, the critical exponents are universal. Applying the cluster approximation to variants of the CP always yields $\beta = 1/2$.

In Figure 8.3, we plot the cluster approximation density *vs.* the series study density. For desorption rates $\lesssim 0.2$ both curves are practically identical. For example, at $\lambda = 0.2$ the relative difference is less than 0.5%. We conclude that despite the failure near the transition point, the cluster approximation is useful in describing the process for a substantial dynamic range. Another way to determine the accuracy of the approximation is by expanding Eq. (8.5) as a power series in λ^n and comparing it to the coefficients obtained by the series expansion study [41]. We find that both expansions are identical to the third order,

$$\rho(\lambda) = \begin{cases} 1 - \lambda - \lambda^2 - 2\lambda^3 - 5\lambda^4 + O(\lambda^5) & \text{CA,} \\ 1 - \lambda - \lambda^2 - 2\lambda^3 - 4\frac{1}{2}\lambda^4 + O(\lambda^5) & \text{CP.} \end{cases} \tag{8.7}$$

Since R_n is of order λ^n, we expect similar correspondence between the approximate interval density from our rate equations and the actual contact process densities. To test this, we have performed a Monte-Carlo simulation with 10^5 particles at $\lambda = 0.2$. Indeed, the average over 200 different realizations yields values for R_n that agree with the approximate density to within 0.5%, for $n = 0, 1, 2, 3$. The quality of the approximation gradually decreases as n increases and for example for $n = 4$ the discrepancy is 4%.

The interval density also exhibits an interesting critical behavior. By expanding the generating function of Eq. (8.4), one finds $R_n = \rho\lambda^n(2n)!/n!(n+1)!$ for $\lambda \leq \lambda_c$. This expression shows that for $\lambda < \lambda_c$ the interval density depends exponentially on the interval length,

$$R_n \sim n^{-3/2} \exp\Big(-4\Delta n\Big) \qquad \Delta \ll 1, \tag{8.8}$$

where $\Delta = \lambda_c - \lambda$. The Stirling formula was used to obtain the above form of the interval density. At the critical point, power-law decay is recovered, $R_n \sim n^{-3/2}$.

8.2 Critical Slowing Down

These static properties are closely related to the kinetics of the system. Far from the critical point, the density rapidly relaxes to its steady-state value from any initial conditions. As the system approaches the critical point, the relaxation time diverges, and a power-law decay of the concentration takes place. We thus expect that for sufficiently large times and close enough to the critical point, the temporal approach to the final state is given by the scaling form [9, 40]

$$\rho - \rho_c \sim t^{-\delta}\psi(\Delta t^{1/\nu}). \tag{8.9}$$

-bb-error = =

Figure 8.4: The critical approach towards the steady-state. Numeric solution to the rate equations (dots) for the case $\lambda = \lambda_c = 1/4$ is plotted. For comparison a line of slope $-1/3$ is also shown (solid).

In other words, the critical exponent δ characterizes the critical kinetics, while the exponent ν characterizes the sub-critical relaxation time. The above scaling form should match the steady-state form of Eq. (8.6) at large times and hence we conclude that $\psi(x) \sim x^\beta$ for $x \gg 1$. To cancel the temporal dependence, the scaling relation $\beta = \delta\nu$ must be satisfied. Furthermore, Eq. (8.8) indicates that the relaxation length associated with the steady-state interval density diverges as $1/\Delta$ as the system approaches the critical point. Thus, it is natural to assume that $R_n(t)$ depends on time through a rescaled size, $n \to nt^{-\alpha}$, as well as a rescaled adsorption rate. Noting that $R_0 = \rho$, we postulate the following scaling behavior for $R_n(t)$:

$$R_n(t) \sim \phi\Big(\Delta t^{1/\nu}, nt^{-\alpha}\Big). \tag{8.10}$$

On the other hand, Eq. (8.8) indicates that the steady-state density depends on the size and the rate only through the variable $n\Delta$. Hence, $\phi(x, y) \sim \tilde{\phi}(xy)$, and by eliminating the temporal dependence we find the scaling relation $\alpha\nu = 1$.

Thus far, our scaling analysis involved matching the anticipated kinetic behavior to the exact steady-state properties. To determine the critical temporal decay, $\rho - \rho_c \sim t^{-\delta}$, we study the rate equations at $\lambda_c = 1/4$. Using the duality relations

	β	δ	ν
CP	0.277	0.160	1.735
CA	1/2	1/3	3/2
SMF	1	1	1

Table 8.1: Static and Critical decay exponents obtained by series studies (CP), Cluster Approximations (CA) and Site Mean-Field (SMF).

between E_n and R_n (see Eq. (8.1)), the rate equations for $\lambda = \lambda_c$ can be rewritten in terms of R_n only,

$$\sum_{l=0}^{n-1} \frac{dR_l}{dt} = \frac{1}{4R_0} \sum_{l=0}^{n-1} R_l R_{n-1-l} - R_n. \tag{8.11}$$

To analyze this equation by scaling techniques, we match the leading asymptotic terms in both sides of the above equation. The left hand side is governed by n terms of order R_n. Hence, by taking into account the time derivative, we conclude that the left hand side is proportional to nR_n/t. The right hand side is dominated by the first few terms in the expansion, namely $l \ll n$ and $n - l \ll n$. Therefore, we approximate the sum by $2R_n(R_0 + R_1 + \cdots)/R_0 = 2R_n/R_0$, using the normalization condition of Eq. (8.2). Finally, we write the resulting expression $R_n\left(1 - 1/2R_0(t)\right)$ in terms of the concentration,

$$\frac{n}{t} R_n \propto R_n(\rho - \rho_c). \tag{8.12}$$

We conclude that $nt^{-1} \sim t^{\alpha - 1} \sim t^{-\delta}$, or equivalently $\alpha + \delta = 1$. The three scaling relations yield the following exponents, $\delta = 1/3$, $\nu = 3/2$ and $\alpha = 2/3$. Numerical integration of the rate equation at $\lambda = \lambda_c$ confirms the scaling prediction for δ (see Figure 8.4). In Table 8.1, we compare the exponents, that result from our cluster approximation (CA), with the corresponding series expansion and the SMF values. We conclude that the CA exponents provide significant improvement in comparison with those from SMF.

Recently, several variants of the CP where introduced and it was shown that they belong to the same universality class as the original model. In these models, the adsorption process is modified while the desorption process remains unchanged. The adsorption rate is set to $\theta/2$ if only one neighboring site is occupied, while the rate remains unity if both neighboring sites are occupied. The empty interval method can be easily generalized to this case, and we merely quote the resulting subcritical steady state density

$$\rho = \frac{\theta + \sqrt{\theta^2 - 4\lambda(\theta-\eta)}}{2(\theta-\eta)}, \qquad \text{with} \qquad \eta = \frac{\lambda(1-\theta)(\theta-2\lambda)}{\theta^2 + (1-\theta)(\theta-2\lambda)}. \tag{8.13}$$

For the basic CP, $\theta = 1$, we recover Eq. (8.5). Clearly, the discontinuous nature of the transition is independent of the microscopic details of the model and the exponent $\beta = 1/2$ is indeed robust. The critical point, however, depends on θ and can be found by equating the square root in Eq. (8.13) to zero. If the adsorption rates are independent of the number of neighboring particles, $\theta = 2$, the predicted critical point is $\lambda_c \cong 0.4608$, while series studies yield $\lambda_c \cong 0.574$ for this so-called A model. In the case where $\theta = 1/2$ (the N3 model), the critical point is $\lambda_c = 0.1366$, while series studies yield $\lambda_c = 0.162$. For the general θ case, the cluster approach yields less accurate estimates for the concentration than for basic CP.

In summary, we have presented an approximate approach to the contact process. Based on the assumption that neighboring empty intervals are not correlated, we solved for the steady state properties. In addition, the kinetic approach towards the steady state was found by scaling techniques. The above approximation is valid for a significant subcritical range. The cluster approximation predicts a discontinuous transition but gives improved exponents in comparison with simple site mean-field theory.

The cluster approximation can be systematically improved by considering higher order interval densities. Indeed, our preliminary results indicate that the second order cluster approximation yields a continuous phase transition. Moreover, the approximation appears to be valid over a significantly larger range of desorption rates.

Chapter 9

Conclusions

In this thesis, I studied several stochastic reaction and adsorption processes and focused mainly on their temporal evolution. These processes usually involved a short-range interaction between the particles. In nearly all cases of interest, the kinetic properties are governed by the long-time spatial structure of the system. In the ballistic annihilation and aggregation processes, particles that move with similar relative velocities tend to survive longer. This leads to the formation of domains of particles moving with similar velocities. Moreover, in the asynchronous ballistic annihilation case, the system organizes according to two distinct interaction lengths. The diffusive interaction length describes the range over which particles moving with the same velocity interact, while the ballistic interaction length controls the length over which opposite-velocity particles interact.

I also studied two nonequilibrium adsorption-desorption processes where collective behavior governs the asymptotic nature. In the case of the parking problem, a consecutive adsorption process leads to slow relaxation kinetics in the desorption controlled limit. On the other hand, for the contact process, the cluster approximation technique manifests the long-range correlations that govern the critical behavior.

Thus, the above processes exhibit nontrivial asymptotic kinetic behavior due to the spatial organization of the particles. I conclude that long time kinetics and the spatial structure are dual properties for a large class of nonequilibrium processes.

Appendix A

The Pair Correlation Function

The pair correlation function satisfies the set of equations

$$\frac{\partial r_k(t)}{\partial \alpha t} = -2r_k(t) + \gamma(r_{k-1}(t) + r_{k+1}(t)), \tag{A.1}$$

for $k \neq 0$ under the boundary condition $r_0 = 1$ (see Eq. (2.8)). As a preliminary step, we solve the above equation under the initial conditions $r_n(t = 0) = \delta_{nl}$. To this end we define the generating function $R(z, t)$ as

$$R(z, t) = \sum_{k=0}^{\infty} r_k(t) z^k. \tag{A.2}$$

The initial conditions yield $F(z, 0) = z^l$. Summation of the rate equations (A.1) gives the following differential equation,

$$\frac{\partial R(z, t)}{\partial \alpha t} = \Big(\gamma(z + z^{-1}) - 2\Big) R(z, t). \tag{A.3}$$

With the above initial conditions, the generating function is found to be

$$F(z, t) = z^n \exp\Big((\gamma(z + z^{-1}) - 2)\alpha t\Big). \tag{A.4}$$

Using the fact that the z-dependent part of the exponent is the generating function of the modified Bessel function $I_n(t)$, expansion of the exponent in terms of these Bessel functions yields

$$r_n(t) = \exp(-2\alpha t) I_{n-l}(2\alpha\gamma t). \tag{A.5}$$

We note that the equilibrium solution to Eq. (A.1) is given by the simple ansatz $r_k^{eq} = \eta^k$, with $2\gamma = (\eta + \eta^{-1})$. Since the rate equations are linear, a solution to the rate equations is given as the sum of the equilibrium correlation and the solution to the time dependent problem. Hence, the problem is reduced to solving Eq. (A.1) for the variables $\tilde{r}_k(t) = r_k(t) - r_k^{eq}$ with a modified boundary condition $\tilde{r}_0(t) = 0$. The image method can be invoked now to ensure vanishing of $\tilde{r}_0$ at all times. For every initial "charge" $\tilde{r}_n(0)$ at positive sites, an equal in magnitude and opposite in sign charge is placed at the site $-n$. The modified spin correlation function is given as a superposition of terms found in Eq. (A.5), and consequently one finds

$$r_k(t) = \eta^k + \exp(-2\alpha t) \sum_{l=1} \Big(r_l(0) - \eta^l \Big) \Big(I_{k-l}(2\alpha\gamma t) - I_{k+l}(2\alpha\gamma t) \Big). \tag{A.6}$$

Appendix B

One-Dimensional Random Sequential Adsorption

In this appendix, we derive a solution to the one-dimensional random sequential adsorption problem, discussed in section 2.3. The general k-mer adsorption is generalized to obtain the continuous case result. In the RSA process, k-mers land uniformly on an initially empty lattice with a constant rate, to be taken as unity without loss of generality. An adsorption event is successful if all k sites are empty. Let $E_n(t)$ denote the probability that n consecutive lattice sites are empty. The rate equations for these probabilities are

$$\frac{dE_n(t)}{dt} = -(n-k+1)E_n(t) - 2\sum_{j=1}^{k-1} E_{j+n}(t) \tag{B.1}$$

for $n \geq k$. The first term in the right-hand side describes adsorption events inside the original n-site sequence. The next terms describe desorption events involving sites outside the original sequence.

Since we start with an empty lattice, $E_n(0) = 1$. Solving Eq. (B.1) subject to these initial conditions yields,

$$E_n(t) = \exp\Big[-(n-k+1)t - 2\sum_{j=1}^{k-1} \frac{1-e^{-jt}}{j}\Big]. \tag{B.2}$$

Similarly, one can write rate equations and solve them exactly for the probabilities $E_n(t)$ with $n < k$. The most interesting quantity, $E_1(t)$, satisfies the equation

$$\frac{dE_1(t)}{dt} = -kE_k(t), \tag{B.3}$$

which involves only $E_k(t)$. By integrating of Eq. (B.3), we find the coverage $c(t)$, $c(t) = 1 - E_1(t)$,

$$c(t) = k\int_0^t dt' \exp\Big[-t' - 2\sum_{j=1}^{k-1}\frac{1-e^{-jt'}}{j}\Big] \tag{B.4}$$

The jamming coverage, $c_\infty \equiv \lim_{t\to\infty} c(t)$, for the case of dimer deposition, $k = 2$, is obtained from Eq. (B.4),

$$c_\infty = 1 - e^{-2}. \tag{B.5}$$

The exact k-mer solution can be used to obtain the continuum limit. In this limit, objects of unit length are deposited without overlapping on a line. To attain this limit we rescale the time $kt \to t$. Thus, we take the limit $k \to \infty$ of Eq. (B.4), with the rescaled time remaining finite, and obtain the following continuum coverage function

$$\rho(t) = \int_0^t dt' \exp\Big[-2\int_0^{t'} du \frac{1-e^{-u}}{u}\Big]. \tag{B.6}$$

When $t \to \infty$, the jamming density approaches the well known Rényi number $\rho_\infty = 0.747597$.

Using the exact solution for the density, we study the approach to the jamming limit. In the lattice case we find from Eq. (B.4) an exponential approach $c_\infty - c(t) \sim \exp(-t)$. Interestingly, in the continuum case the approach is much slower. By differentiation of Eq. (B.6) with respect to time and by keeping the leading orders in the Exponential Integral $\int_0^t du(1-e^{-u})/u \cong -\gamma - \ln t$, the asymptotic approach to the jammed coverage is found

$$\rho_\infty - \rho(t) \sim \frac{e^{-2\gamma}}{t}, \tag{B.7}$$

where $\gamma = 0.5772$ is the Euler constant.

Appendix C

The Cumulative Velocity-Size Distribution

In this appendix, we describe the derivation leading to the asymptotic form of the cumulative velocity-size distribution. The resulting expression is valid for any initial velocity distribution which obeys a power-law for small velocities. The starting point for calculating of $Q_m(v,t)$ is the formal expression of Eq. (3.24). By interchanging the order of the velocity and space integrations, this expression can be rewritten as

$$Q_m(v,t) = P(v,t) \prod_{i=1}^{m-1} \int_0^\infty dx_i \exp(-x_i) \int_{v+(x_1+\cdots+x_i)/t}^\infty dv_i \, P_0(v_i). \tag{C.1}$$

Since the details of the initial distribution for large velocities do not change the form of the scaling solution, we may treat the more general power-law case by choosing a specific initial distribution of velocities whose form is convenient for performing the integration over the velocity in the right-hand side of Eq. (C.1). Since the velocity distribution near $v = 0$ has a power-law tail, the most convenient initial distribution is

$$P_0(v) = av^\mu \exp\left(-av^{\mu+1}/(\mu+1)\right). \tag{C.2}$$

For the specific initial velocity distribution of Eq. (C.2), the integration over the velocity variables is immediate, and one finds

$$Q_m(v,t) = P(v,t)\prod_{i=1}^{m-1}\int_0^\infty dx_i \exp(-x_i)\exp\left[-a\Big(v+(x_1+\cdots+x_i)/t\Big)^{\mu+1}/(\mu+1)\right]. \tag{C.3}$$

To evaluate the multiple spatial integration, we note that the argument $\Big(v+(x_1+\cdots+x_i)/t\Big)$ decays to zero. It can be treated as a small correction. The integral in Eq. (C.3) can be estimated using the following asymptotic relation,

$$\prod_{i=1}^{m-1}\int_0^\infty dx_i e^{-x_i} f(v+\epsilon(x_1+\cdots+x_i)) = \prod_{i=1}^{m-1} f(v+\epsilon i) + O(\epsilon^2). \tag{C.4}$$

This relation is obtained by expanding f as a first order Taylor series in the vicinity of $z = v$. The spatial integration is carried out by noting that the first moment of a simple decaying exponential factor equals unity. The resulting expression is recognized as $f(v+\epsilon i)$. The integration procedure is then iterated for $i = 1, \cdots, m-1$. The correction to the argument v is bounded by $n/t \sim t^{-\beta}$, and therefore, by choosing $\epsilon = 1/t$, Eq. (C.4) is valid for performing the spatial integrations in Eq. (C.3). By substituting the explicit functional form, $f(z) = \exp(-bz^{\mu+1}/(\mu+1))$, we have

$$Q_m(v,t) = P(v,t)\prod_{i=1}^{m-1}\exp\Big(-a(v+i/t)^{\mu+1}/(\mu+1)\Big). \tag{C.5}$$

Finally, the product of the exponential factors is written as an exponent of a sum. In the limit of large n, this sum is equivalent to the integral $a\int_0^{m-1} dy(v+y/t)^{\mu+1}/(\mu+1)$. Evaluating this integral, the asymptotic form of the cumulant mass-velocity density is obtained as

$$Q_m(v,t) \simeq av^\mu \exp\left[-b(vt^\beta + mt^{-\alpha})^{\mu+2}\right]. \tag{C.6}$$

In evaluating this asymptotic expression, the exponential factor of $P(v,t)$ cancels the factor that emerges from the lower limit of the integration over y. In Eq. (3.24), the above expression is written as a scaling function.

Appendix D

Computation of the Time Series

In this appendix, we detail the computation of the coefficients of the time series representation of the concentration of a specific species. As discussed in chapter 5, the evolution operator $\mathcal{L}$ is applied to the initial state n times to obtain the first n terms of the state function of Eq. (5.8). To minimize the computation, it is useful to work with a ring of length $n+1$. For a process involving m distinct species, each site can take on $m+1$ possible values (including the empty site). We label each species by an index i, $i = 1, 2, \ldots, m$, and label the empty site by $i = 0$. A k-site configuration can therefore be labeled by its k-digit $m+1$-base representation. For example, the configuration, $|AOAA\rangle$ in base 2 is labeled by $1 \times 2^3 + 0 \times 2^2 + 1 \times 2^1 + 1 \times 2^0 = 11$. The initial state for homogeneous systems is often chosen as the state where each site is occupied with a randomly chosen species. This state is a superposition of all m^k configurations and is divided by m^k to ensure unit normalization. The application of the operator $\mathcal{L} = \mathcal{L}_{AO} + \mathcal{L}_{OA} + \mathcal{L}_{AA}$ is made term-by-term. The right-hop operator $\mathcal{L}_{AO}$ acts only on the two-site segments $|AO\rangle$, and for example $\mathcal{L}_{AO}|AOAA\rangle = |OAAA\rangle - |AOAA\rangle$. In the integer representation, a 4×4 matrix represents the action of the operator $\mathcal{L}_{AO}$ on any two site segment. For example, $\mathcal{L}_{AO}(2,1) = 1$ and $\mathcal{L}_{AO}(2,2) = -1$, while $\mathcal{L}_{AO}$ vanishes otherwise. After the operator $\mathcal{L}$ is applied once, $|\Psi_0\rangle$, the first term in the expansion of $|\Psi(t)\rangle$ is found. We then obtain c_1, the first term in the expansion of the concentration $c(t) = c_0 + c_1 t + \cdots$, by evaluating the expectation value of the

A species concentration operator of Eq.(6.10). This procedure is repeated until the n^{th} coefficient is found.

To minimize the computation, it is convenient to use the translational reflection symmetries of the evolution operator. For homogeneous processes, translationally invariant configurations of the system can be identified with one representative configuration. The equivalent configurations are taken into account via the multiplicity factor of each representative configuration. The following diagram highlights the computer algorithm, with the main subroutines displayed in bold face.

THE ALGORITHM

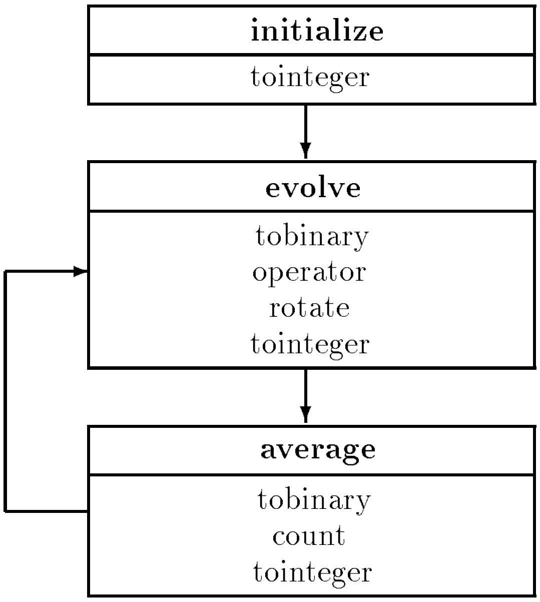

THE SUBROUTINES

initialize	Creates a homogeneous initial state with k species.
evolve	Applies the evolution operator once.
average	Receives a state and counts the expectation value of the A-species concentration operator.

tointeger	Converts an $m+1$-base array representation to an integer number.
tobinary	Converts an integer number to an $m+1$-base array representation.
operator	Receives a particle configuration and acts on each two site segment according to the evolution operator.
rotate	Receives an $m+1$-base array representation, rotates the digits $n+1$ times, and returns the minimal integer representation.
count	Counts the number of A-particles in a given configuration.

Bibliography

[1] E. Ising, *Z. Phys.* **31**, 253 (1925).

[2] L. Onsager, *Phys. Rev.* **65**, 117 (1944).

[3] R. J. Glauber, *J. Math. Phys.* **4**, 294 (1963).

[4] A. A. Lushnikov, *Sov. Phys. JETP* **64**, 811 (1986).

[5] J. L. Spouge *Phys. Rev. Lett.* **60**, 871 (1988).

[6] D. ben-Avraham, M. A. Burschka and C. R. Doering, *J. Stat. Phys.* **60**, 695 (1990).

[7] R. Kroon, H. Fleurent, and R. Sprik, *Phys. Rev. E* **47**, 2462 (1993).

[8] P. Nielaba and V. Privman, *Mod. Phys. Lett. B* **9**, 533 (1992).

[9] Z. Racz, *Phys. Rev. Lett.* **55**, 1707 (1985).

[10] P. J. Flory, *J. Am. Chem. Soc.* **61**, 1518 (1939).

[11] Y. Elskens and H. L. Frisch, *Phys. Rev. A* **31**, 3812 (1985).

[12] Ya. B. Zeldovich and A .A. Ovchinnikov, *Chem. Phys.* **28**, 215 (1978).

[13] F. Leyvraz and S. Redner, *Phys. Rev. Lett.* **66**, 2168 (1991).

[14] M. Bramson and J. L. Lebowitz, *J. Stat. Phys.* **65**, 941 (1991).

[15] J. C. McWilliams, *J. Fluid Mech.* **146**, 21 (1984).

[16] G. Wetherill, in *The Formation and Evolution of Planetary Systems* (Cambridge Univ. Press, 1988).

[17] G. F. Carnevale, Y. Pomeau and W. R. Young, *Phys. Rev. Lett.* **64**, 2913 (1990).

[18] Y. Jiang and F. Leyvraz, *J. Phys. A* **26**, L179 (1993).

[19] K. Kang and S. Redner, *Phys. Rev. A* **32**, 435 (1985).

[20] G. Zumofen, A. Blumen, and J. Klafter, *J. Chem. Phys.* **82**, 3198 (1985).

[21] F. Leyvraz and S. Redner, *Phys. Rev. A* **46**, 3132 (1992).

[22] Z. Vardeny, P. O'Conner, S. Ray and J. Tauc, *Phys. Rev. Lett.* **44**, 1267 (1980).

[23] R. Kopelman, C. S. Li and Z. Y. Shi, *J. Lum.* **45**, 40 (1990).

[24] F. Leyvraz, (private communication, 1993).

[25] P. L. Krapivsky, (private communication, 1993).

[26] N. H. Gartner and N. H. M. Wilson, *Transportation and Traffic Theory*, (Elsevier, New York, 1987).

[27] W. Leutzbach, *Introduction to the Theory of Traffic Flow* (Springer-Verlag, Berlin, 1988).

[28] O. Biham, A. Middleton, and D. Levine, *Phys. Rev. A* **46**, 6124 (1992).

[29] T. Nagatani, *Phys. Rev. E* **48**, 3290 (1993).

[30] A. Schadschneider and M. Schreckenberg, *J. Phys. A* **26**, L679 (1993).

[31] I. Prigogine and R. Herman, *Kinetic Theory of Vehicular Traffic* (Elsevier, New York, 1971).

[32] G. B. Whithem, *Linear and Nonlinear Waves* (Wiley, New York, 1974).

[33] B. S. Kerner and R. Konhauser, *Phys. Rev. E* **48**, 2335 (1993).

[34] E. Ben-Naim, P. L. Krapivsky and S. Redner, submitted to *Phys. Rev. E* (1994).

[35] M. Doi, *J. Phys. A* **9**, 1465; 1479 (1976).

[36] P. Grassberger and M. Scheunert, *Fortschr. Phys.* **28**, 547 (1980).

[37] B. Friedman, G. Levine and B. O'Shaughnessy, *Phys. Rev. A* **46**, 7343 (1992).

[38] M. Droz and L. Savári, *Phys. Rev. E* **48**, 2343 (1993).

[39] B. Lee, *Phys. Rev. E* (1994).

[40] R. Dickman and I. Jensen, *Phys. Rev. Lett.* **67**, 2391 (1991).

[41] I. Jensen and R. Dickman, *J. Stat. Phys.* **71**, 89 (1993).

[42] S. Song and D. Poland, *J. Phys. A* **25**, 3913 (1992).

[43] E. Ben-Naim and J. Zhuo, *Phys. Rev. E* **48**, 2603 (1993).

[44] H. Larralde, Y. Lereah, P. Trunfio, J. Dror, S. Havlin, R. Rosenbaum and H. E. Stanley, *Phys. Rev. Lett.* **70**, 1461 (1993).

[45] L. Gálfi and Z. Rácz, *Phys. Rev. A* **38**, 3151 (1988).

[46] Y -E. L. Koo, L. Li, and R. Kopelman, *Mol. Cryst. Liq. Cryst.* **183**, 187 (1990).

[47] Y. -E. L. Koo and R. Kopelman, *J. Phys. A* **65**, 893 (1991).

[48] S. Redner and D. ben-Avraham, *J. Phys. A* **23**, L1169 (1990).

[49] Z. Jiang and C. Ebner, *Phys. Rev. A* **42**, 7483 (1990).

[50] M. Araujo, S. Havlin, H. Lerralde and H. E. Stanley, *Phys. Rev. Lett.* **68**, 1791 (1992).

[51] S. Cornell and M. Droz, *Phys. Rev. Lett.* **70**, 3824 (1993).

[52] G. Y. Onoda and E. G. Liniger, *Phys. Rev. A* **33**, 715 (1986).

[53] J. W. Evans, *Rev. Mod. Phys.* **65**, 1281 (1993).

[54] D. J. Dwyer, G. W. Simmons and R. P. Wei, *Surf. Sci.* **64**, 617 (1977).

[55] W. Hung, J. Schwartz and S. Bernasek, *Surf. Sci.* **248**, 332 (1991).

[56] J. Feder, *J. Theor. Biol.* **87**, 237 (1980).

[57] Y. Pomeau, *J. Phys. A* **13**, L193 (1980).

[58] R. H. Swedsen, *Phys. Rev. A* **24**, 504 (1981).

[59] E. L. Hinrichsen, J. Feder, and T. Jossang, *J. Stat. Phys.* **44**, 793 (1986).

[60] A. Rényi, *Publ. Math. Inst. Hung. Acad. Sci.* **3**, 109 (1958).

[61] J. J. Gonzalez, P. C. Hemmer, and J. S. Hoye, *Chem. Phys.* **3**, 228 (1974).

[62] P. Schaaf, A. Johner, and J. Talbot, *Phys. Rev. Lett.* **66**, 1603 (1991).

[63] G. Tarjus and P. Viot, *Phys. Rev. Lett.* **68**, 2354 (1992).

[64] V. Privman and M. Barma, *J. Chem. Phys.* **97**, 6714 (1992).

[65] G. Tarjus, P. Schaaf, and J. Talbot, *J. Chem. Phys.* **93**, 8352 (1990).

[66] R. B. Stinchcombe, M. D. Grynberg, and M. Barma, *Phys. Rev. E* **47**, 4018 (1993).

[67] E. R. Cohen and H. Reiss, *J. Chem. Phys.* **38**, 680 (1963).

[68] J. J. Gonzalez and P. C. Hemmer, *J. Chem. Phys.* **67**, 2469 (1977).

[69] J. W. Evans, D. K. Hoffmann, and D. R. Burgess, *J. Chem. Phys.* **80**, 935 (1984).

[70] A. S. Zasedatelev, G. V. Gurskii, and M. V. Volkenshtein, *Molek. Biol.* **5**, 245 (1971).

[71] J. D. McGhee and P. H. von Hippel, *J. Mol. Biol.* **86**, 469 (1974).

[72] T. L. Hill, *Cooperativity Theory in Biochemistry*, (Springer-Verlag, New York, 1985).

[73] T. E. Harris, *Ann. Prob.* **2**, 969 (1974).

[74] T. M. Liggett, *Interacting Particle Systems* (Springer-Verlag, New York, 1985).

[75] F. Schlogl, *Z. Phys. B* **253**, 147 (1972).

[76] J. L. Cardy and R. L. Sugar, *J. Phys. A* **13**, L423 (1980).

[77] W. Kinzel, *Z. Phys. B* **58**, 229 (1985).

[78] R. B. Ziff, E. Gulari and Y. Barshad, *Phys. Rev. Lett.* **56**, 2553 (1986).

[79] H. K. Janssen, *Z. Phys. B* **42**, 151 (1981).

[80] P. Grassberger and A. de la Torre, *Ann. Phys. (N.Y.)* **122**, 373 (1979).

[81] I. Jensen, *Phys. Rev. A* **45**, R563 (1992).